

The Cloverleaf Antenna:
A Compact Wide-bandwidth Dual-polarization Feed for
CHIME

by

Meiling Deng

B.Sc., Huazhong University of Science and Technology, 2012

A THESIS SUBMITTED IN PARTIAL FULFILLMENT OF
THE REQUIREMENTS FOR THE DEGREE OF
MASTER OF SCIENCE

in

The Faculty of Graduate and Postdoctoral Studies
(Astronomy)

THE UNIVERSITY OF BRITISH COLUMBIA
(Vancouver)

August 2014

© Meiling Deng 2014

Abstract

A compact, wide-bandwidth, dual-polarization cloverleaf-shaped antenna has been developed to feed the CHIME radio telescope. The antenna has been tuned using a commercial antenna simulation program, CST, to have a very good impedance match to our amplifiers. Specifically, the return loss is smaller than -10dB for over an octave of bandwidth, covering the full CHIME band from 400MHz to 800MHz and this performance has been confirmed by measurement. The antennas are made of conventional low-loss circuit boards and can be mass produced economically, which is important because CHIME requires 1280 feeds. They are compact enough to be placed 30cm apart in a linear array at any azimuthal rotation. 128 of these feeds have now been built, tested and deployed on CHIME pathfinder.

Preface

A discussion among myself, Mark Halpern and Tom Landecker led to design of my research program, which is to use a commercial software CST to design a wide bandwidth feed for CHIME. Later discussion among myself, Mark Halpern, Tom Landecker and Duncan Campbell-Wilson led to the realization that curved petal shapes in a cloverleaf feed might reduce resonances and produce a broadband feed.

The work in sections 2.1.2, 2.2 and 2.3, which sets the starting point for my search for a CHIME feed, was led by other members of the CHIME collaboration, particularly Gregory Davis and Ivan Padilla. The work in section 6.2 and 6.3 was done in collaboration with the whole CHIME team.

Figures 2.2, 2.3, 2.4, 2.6, 5.7, 6.5 and 6.6 are made by other members of the CHIME team. There are some illustrative figures which are publicly available and in each case, citation is provided in the caption. The rest of work presented in this thesis is done by myself.

The main result of this thesis has been accepted for publication in the proceedings of ANTEM 2014. The accepted paper is in appendix. (The Cloverleaf Antenna: A Compact Wide bandwidth Dual-polarization Feed for CHIME; Meiling Deng, Duncan Campbell-Wilson for the CHIME collaboration). I wrote the paper with help from Mark Halpern, Tom Landecker and Duncan Campbell-Wilson. The results were presented there by the author. This work won a prize as the best student paper at the conference.

Table of Contents

| | |
|---|-----|
| Abstract | ii |
| Preface | iii |
| Table of Contents | iv |
| List of Tables | vi |
| List of Figures | vii |
| Acknowledgements | ix |
| 1 Introduction | 1 |
| 1.1 The Existence of Dark Energy | 1 |
| 1.2 Properties of Dark Energy is Measurable | 2 |
| 1.2.1 Baryon Acoustic Oscillations | 3 |
| 1.2.2 21cm Observation | 4 |
| 1.3 Overview of CHIME as A New Dark Energy Experiment | 4 |
| 2 Starting Point for the CHIME Feed Development | 7 |
| 2.1 The Four Square Antenna as the First Candidate for the CHIME Feed | 8 |
| 2.1.1 Working Principles of the 4sq | 9 |
| 2.1.2 CHIME 4sq on the Two Dish System | 11 |
| 2.2 The Active 4sq | 14 |
| 2.3 The Four Point feed and The Four Sleeve feed | 16 |
| 3 Method | 18 |
| 3.1 Grasp | 18 |
| 3.2 CST | 20 |
| 3.2.1 CST Simulation Overview | 20 |
| 3.2.2 Test of our Approach to CST through A Dipole Model | 21 |
| 3.2.3 Plan of Use | 28 |

Table of Contents

| | | |
|----------|---|----|
| 4 | Modeling the Current Patterns, Beam Shapes and Impedance Spectra of Single Feed 4sq and its Variants | 29 |
| 4.1 | Visualizing Current Patterns and Beam Shapes | 29 |
| 4.1.1 | The 4sq and Its Petal board Model | 29 |
| 4.1.2 | 4sq's Variants and Their Petal Board Models | 36 |
| 4.1.3 | Comparison of Different Feeds | 40 |
| 4.2 | Input Impedance of Single 4sq | 41 |
| 4.2.1 | Petal Board Model and Impedance Transformation | 41 |
| 4.2.2 | Full Feed Model | 51 |
| 5 | The Cloverleaf Feed | 53 |
| 5.1 | Inspiration and Confirmation of the Cloverleaf Idea | 53 |
| 5.2 | CHIME Cloverleaf Feed | 54 |
| 5.2.1 | Further Test of the Full Feed Model | 54 |
| 5.2.2 | Cloverleaf Feed Design and Optimization | 55 |
| 5.2.3 | Realization of the Optimized Cloverleaf Feed Design | 57 |
| 6 | Manufacture and Deployment of The Cloverleaf Feeds | 61 |
| 6.1 | Specifications of the Designed Cloverleaf Feed | 61 |
| 6.2 | Manufacture Process | 63 |
| 6.3 | Sky Data Taken from Deployed Cloverleaf Feeds | 66 |
| 7 | Conclusion | 70 |
| | Bibliography | 72 |
| | Appendix | 73 |

List of Tables

| | | |
|-----|--|----|
| 3.1 | Input impedance comparison for half-wavelength dipole for different values of rN , while fixing $gN=100$ | 28 |
| 4.1 | HPBW comparison among the 4sq, 4pt and 4sl. | 41 |
| 5.1 | Designed parameters of the cloverleaf feed in CHIME band. | 57 |
| 6.1 | Details on The Cloverleaf Feeds' Acceptance Test. | 63 |

List of Figures

| | | |
|------|---|----|
| 1.1 | Evolution history of the universe | 2 |
| 1.2 | Hyperfine splitting of neutral hydrogen | 4 |
| 1.3 | The CHIME reflector | 6 |
| 2.1 | Structure of the 4sq antenna | 9 |
| 2.2 | A diagram to illustrate how the 4sq feed is balanced | 10 |
| 2.3 | A diagram to illustrate the general idea of in-pair feeding | 11 |
| 2.4 | Measured performance of the CHIME 4sq | 13 |
| 2.5 | The active 4sq | 14 |
| 2.6 | Measured beam of the active 4sq | 15 |
| 2.7 | The 4pt built as a modification of the 4sq | 16 |
| 2.8 | The 4sl built as a modification of the 4sq | 17 |
| 3.1 | A simple example of Grasp model | 19 |
| 3.2 | Dipole antenna | 21 |
| 3.3 | The dipole model setup in CST | 24 |
| 3.4 | Currents of the half-wavelength dipole simulated by CST | 26 |
| 3.5 | Comparison of dipole's current distributions among CST FDTD, python MoM and analytical solution | 27 |
| 4.1 | Petal board model of the 4sq in CST | 30 |
| 4.2 | Simulated current pattern of the 4sq | 31 |
| 4.3 | Bent dipole model for representation of the 4sq | 32 |
| 4.4 | Simulated 3D beam pattern of the 4sq at 600 MHz | 33 |
| 4.5 | Simulated E plane and H plane of the 4sq | 34 |
| 4.6 | H plane's beam width comparison between simulation and measurement | 35 |
| 4.7 | the 4pt petal board model | 37 |
| 4.8 | Simulated beam pattern of the 4pt at 600 MHz | 38 |
| 4.9 | The 4sl petal board model | 39 |
| 4.10 | Beam pattern of the 4sl at 600 MHz | 40 |
| 4.11 | Diagram of a transmission line and its lumped circuit model | 42 |

List of Figures

| | | |
|------|--|----|
| 4.12 | Diagram of impedance transformation of the transmission line | 44 |
| 4.13 | Return loss comparison between impedance transformation method and measurement | 46 |
| 4.14 | Z_{in} of a single short-ended microstrip transmission line | 47 |
| 4.15 | A model of 4sq's petal board fed by only one microstrip transmission line | 49 |
| 4.16 | Input impedance comparison between direct simulation and impedance transformation in the context of one microstrip feeding the 4sq petal board | 50 |
| 4.17 | Full feed model of the 4sq | 51 |
| 4.18 | Return loss comparison between full 4sq model simulation and measurement | 52 |
| | | |
| 5.1 | A cloverleaf prototype in MOST band | 54 |
| 5.2 | A cloverleaf prototype in CHIME band | 55 |
| 5.3 | Parametrization of petal shape of the cloverleaf antenna | 56 |
| 5.4 | A three-stage transmission line for the cloverleaf antenna | 57 |
| 5.5 | The cloverleaf feed built according to the designed parameters | 58 |
| 5.6 | Return loss comparison between measurement and simulation of the CHIME cloverleaf feed | 59 |
| 5.7 | Measured beam pattern of CHIME cloverleaf feed | 60 |
| | | |
| 6.1 | Annotations to manufacture the cloverleaf feed | 62 |
| 6.2 | Panelization of the base boards and stem boards | 64 |
| 6.3 | A jig for assembling the cloverleaf feeds | 65 |
| 6.4 | The cloverleaf feeds installed on CHIME pathfinder | 65 |
| 6.5 | One pulse measurement of the pulsar B0329+54 from the cloverleaf feed on CHIME pathfinder | 66 |
| 6.6 | Holography to measure a slice of reflector beam | 68 |
| 6.7 | Grasp simulation of reflector beam and its comparison to measurement in terms of beam width | 69 |

Acknowledgements

I would like to thank MITACS for their financial support during my master program. I would like to thank many people at DRAO for their support. I am very grateful for all the help I received from the CHIME team and I feel honored to work with CHIME. I want to say sincere thanks to Mandana Amiri, Gregory Davis, Don Wiebe, Mateus Fandino, Rick Smegal and Tom Felton who help me with great patience and long-term support. I would like to say many thanks to Gary Hinshaw for his patience, encouragement and guidance. I am very appreciative of all the help, advice and insight I got from my supervisor Mark Halpern. At last but not least, I want to say sincere thanks to Yang Lan who helped through my whole master program with great patience, encouragement, problem-solving and devotion.

Chapter 1

Introduction

The Canadian Hydrogen Intensity Mapping Experiment (CHIME)¹ [1] is an ongoing interferometric radio experiment to measure properties of dark energy. In particular, CHIME will map neutral hydrogen distribution by observing the 21cm hyperfine transition line in the redshift range $0.8 < z < 2.5$.

1.1 The Existence of Dark Energy

Fig. 1.1 shows the evolution history of the universe. The far left is the earliest moment we can now probe, when a period named inflation is hypothesized to have produced a burst of exponential growth of the universe's size. At the end of inflation, there are photons, electrons, protons, neutrons, neutrinos, dark matter and other form of energy. Photons interact very rapidly with charged particles so they are trapped in this hot, dense plasma. As time goes on, the universe cools down because of expansion. When the universe's temperature cools down to ~ 3000 K, electrons and protons begin joining together to form neutral hydrogen. This process frees photons and makes its free path almost size of the universe. This era is called recombination. The released photons forms Cosmic Microwave Background (CMB), which can be seen today from every direction with a temperature 2.7 K.

Later on, local neutral hydrogen condenses due to attractive gravitational force. The core of those condensed neutral hydrogen has higher and higher temperature and pressure, which ignites nuclear reaction. These are the first stars generated. As time goes on, local stars get closer to each other to form first galaxies due to attractive gravitational force again. During this whole process, expansion of the universe is decelerating because attractive gravitational force is the only long-distance force.

What is very strange is that, during the development of galaxies, expansion begins to accelerate. A direct measurement to support this acceleration comes from supernovae observation by measuring their luminosity distances

¹<http://phas.ubc.ca/chime>

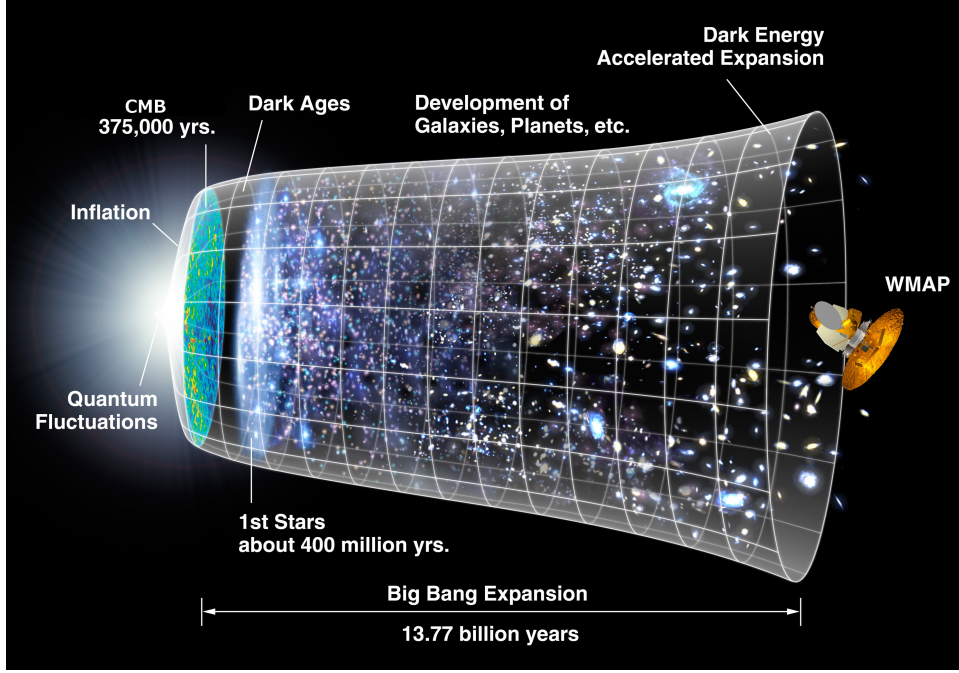


Figure 1.1: A figure to illustrate the evolution history of the universe over 13.7 billion years. Time evolves in the horizontal direction. 3D universe at a time is depicted by a cross section of the grid. Image credit: NASA/WMAP Science Team.

[2, 3]. A model to explain this acceleration is dark energy (DE) [4]. Define w to be $w \equiv \frac{P}{\rho}$, where P is pressure and ρ is the energy density. For normal matter, pressure is negligible, so $w \approx 0$. For radiation, $w = \frac{1}{3}$. By solving the Einstein equations, the energy density of dark energy evolves like:

$$\rho_{DE} \propto \exp\left\{-3 \int^a \frac{da'}{a'} [1 + w(a')]\right\}, \quad (1.1)$$

where a is size of the universe if size of the universe today is defined to be 1. Among all possible values of w , $w_{DE} = -1$, which indicates constant dark energy density through expansion, is consistent with data [5, 6].

1.2 Properties of Dark Energy is Measurable

As indicated above, properties of dark energy has not been uniquely decided from the existing observations. Among different models of dark energy, there

are distinct predictions of expansion history, especially in the redshift range $0.8 < z < 2.5$, which is the range that CHIME wants to measure. The redshift, z , is defined as

$$z + 1 \equiv \frac{\lambda_{observed}}{\lambda_{emitted}} = \frac{1}{a}, \quad (1.2)$$

where $\lambda_{emitted}$ is the wavelength of a signal when it was emitted, $\lambda_{observed}$ is wavelength of a signal when it is later observed.

1.2.1 Baryon Acoustic Oscillations

Before recombination, photons and charged matter (electrons and protons) are coupled to each other due to Compton scattering. The universe is like a very hot, dense, simple plasma, but it is not absolutely evenly distributed. An over dense spot can be initialized by quantum fluctuations. Attractive gravitational force tends to strengthen this over dense spot, while interaction between photons and charged particles generates heat and creates outward pressure. The counteracting inward gravitation and outward pressure create oscillations, which are called Baryon Acoustic Oscillations (BAO). These oscillations result in an outgoing spherical wave from the over dense spot. Charged particles and photons travel together with this spherical wave while dark matter stays in the over dense spot because it interacts only gravitationally. The spherical wave keeps going outward until recombination of electrons and protons frees photons from them and releases pressure from the whole system. From then on, photons travel freely in space, while the combined neutral hydrogen stays on the spherical shell and keeps attracting local matter to the shell due to gravitation. Therefore, a special pattern of matter distribution is formed and strengthened. The radius of the spherical shell is called sound horizon, whose size only changes proportionally to size of the universe. In fact, lots of over dense spots were generated before the recombination. Therefore, it is not one spherical shell in the universe but an interference of many of them, like the pattern in a pond with many raindrops.

Measuring the two point correlation function across a large section of sky would reveal BAO pattern statistically. Therefore BAO can be used as a standard ruler because comparison of its angular size to its redshift constitutes a measurement of the expansion history, given that its comoving size is known from CMB measurement to be 150 Mpc.

1.2.2 21cm Observation

BAO can be seen in the neutral hydrogen distribution because neutral hydrogen traces the matter distribution on large scales. A key feature of neutral hydrogen to make BAO measurement possible is that the neutral hydrogen emits or absorbs radio wave at 1420 MHz due to hyperfine splitting of its atomic energy level, which is shown in Fig. 1.2. This radio wave is called HI emission or 21cm signal. In the redshift range $0.8 < z < 2.5$, apparent frequency of HI emission will be redshifted to the range $(400\text{MHz}, 800\text{MHz})$. Therefore, measuring 21cm signal as a function of frequency is to measure the matter distribution as a function of redshift. CHIME's frequency resolution is set to around 0.5 MHz, which is much finer than 10 MHz frequency resolution required to resolve BAO scale to its third harmonics.

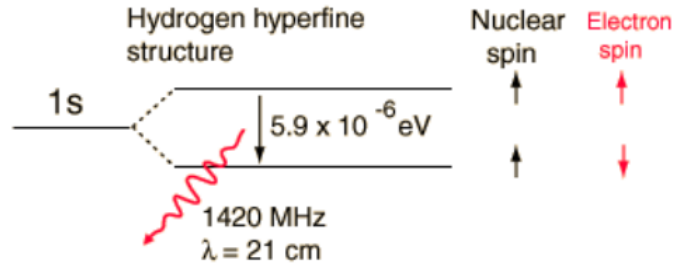


Figure 1.2: Hyperfine splitting of neutral hydrogen corresponding to 21cm transition. Image source: <http://hyperphysics.phy-astr.gsu.edu/hbase/quantum/h21.html>

One of the biggest challenge in 21cm observations is to remove foreground contamination, which is a thousand times brighter than the 21cm signal. The foreground removal strategy [7] is based on the fact that 21cm signal is not a smooth function of in frequency because of large scale structure in the universe while foreground signals from galaxies or point radio sources are all smooth.

1.3 Overview of CHIME as A New Dark Energy Experiment

The proposed CHIME consists of five cylindrical reflectors with no moving parts, as shown in Fig. 1.3 (a). Each of them is 20 m wide, 100 m long and 5

m high at focus. It will drift scan northern half of the sky every day because of earth's self rotation. Half of the sky measurement in the redshift range $0.8 < z < 2.5$ corresponds to a survey volume around $203(h^{-1}Gpc)^3$, in which both angular size and radial size of BAO can be resolved. CHIME's large survey volume is important for measuring BAO statistically. In addition, cylindrical reflectors cost much less compared with dishes since cylindrical reflectors are curved in only one dimension.

To measure the universe's expansion history around $0.8 < z < 2.5$, CHIME needs to invent specialized feed deployed as element of feed array on the focal line of reflectors. Specialized feed designed for CHIME is the topic of this thesis. CHIME needs to invent cheap Low Noise Amplifier (LNA) [8], which is right after the feed element in the analog chain. CHIME also needs to invent digital FX correlator after the analog chain to do Fourier transformation and product correlation of large amount of data.

CHIME Pathfinder

Before implementation of the full CHIME, CHIME pathfinder has been built. The CHIME pathfinder consists of 2 cylindrical reflectors, each of them to be 20 m wide and 36.8 m long, at the site of DRAO, as shown in Fig. 1.3 (b). Signals are received from sky through feeds on the focal line and then amplified by the LNA. Coax cables are used to transport signal from focal line to the C-Can, which is an Radio Frequency (RF) shielded room. Filters are followed to get signal in the 400 MHz to 800 MHz range. Then with appropriate attenuators, analog signals are digitalized by the Analog to Digit Converter (ADC), then Fourier transformed and correlated by FX correlator for data manipulation and analysis. This chain of CHIME pathfinder is almost the same as that of the full CHIME. Therefore, the pathfinder is a fairly good representative of the full CHIME so that it can be used for seeking answers of some crucial questions.

Several examples of those crucial questions are:

- Does the current design of feed and reflector give the beam that can be used to extract scientific signals?
- Are the gain and phase of the LNA stable enough or at least tractable?
- Does the FX correlator work as what we hope?
- Can the overall system be calibrated?
- Shall we use beamforming or N^2 correlation as the calibration strategy?

1.3. Overview of CHIME as A New Dark Energy Experiment

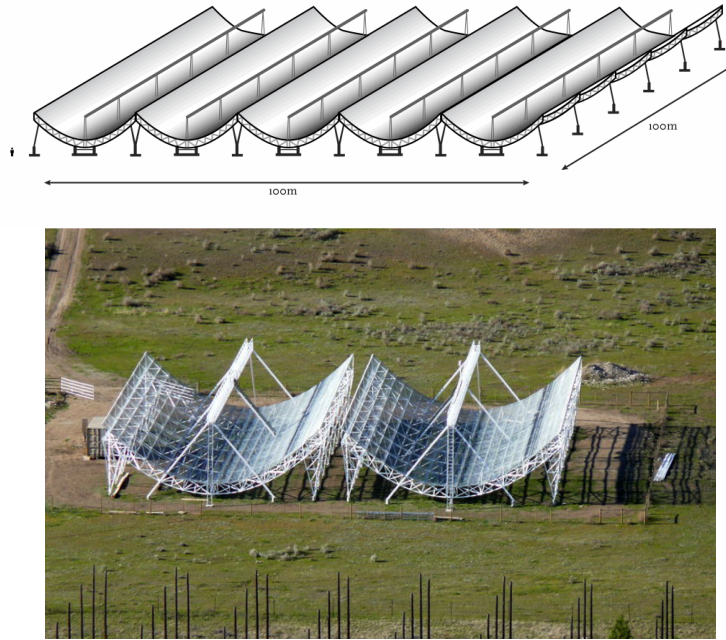


Figure 1.3: (a) Reflectors of the proposed full CHIME. (b) A picture of the CHIME pathfinder at the DRAO site.

Chapter 2

Starting Point for the CHIME Feed Development

CHIME will use linear arrays of antennas placed along the focal line of each cylindrical reflector to examine extremely weak signals. To optimize the Signal to Noise Ratio (SNR) of this measurement, the antennas must efficiently transmit astronomical signals to the first stage amplifiers, which is LNA, while introducing only minimal noise to the system. Therefore each individual antenna must have the following properties.

1. The feed needs to have smaller than -10dB Return Loss (RL)² across 400-800 MHz range, where RL is defined as

$$RL \equiv 10\log_{10}\frac{P_{ref}}{P_{in}} = 20\log_{10}|\Gamma|. \quad (2.1)$$

P_{ref} is the reflected power, P_{in} is the incident power and Γ is the reflection coefficient due to impedance mismatch between feed and LNA.

2. The feed needs to have two polarizations to fully measure the incident fields.
3. To make full use of the reflector surface, CHIME feed needs to have wide beam pattern because the focal line's angle to the EW edges of reflector is 90 degree and angle to the NS edges of reflector is 86 degree.
4. Size of each element should be small enough so that it can be placed into the feed array which has 30 cm separation between elements.
5. The feed should be low-cost and highly repeatable to be mass produced because the full CHIME is going to deploy 1280 feeds in total.
6. Location of phase center of all frequencies must be the same.

²Here the dB expression of return loss is defined to be negative. The smaller the return loss, the smaller the reflected power. In some cases, the dB expression of return loss might be defined to be positive as $-10\log_{10}\frac{P_{ref}}{P_{in}}$

7. The feed must be low-loss to reduce system noise.

The first requirement is there because low return loss results in high SNR, which is an important parameter to describe the efficiency of an experiment. SNR of CHIME is

$$SNR = \frac{T_{sky,measured}}{T_{sys}} = \frac{T_{sky}(1 - |\Gamma|^2)}{T_{sys}} = \frac{T_{sky}}{T_{sys}/(1 - |\Gamma|^2)}, \quad (2.2)$$

where $T_{sys}/(1 - |\Gamma|^2)$ is the effective system temperature. The existence of mismatch between feed and LNA results in higher effective system temperature. In the case of CHIME, T_{sys} is around 50 K, so that -5 dB return loss of feeds results in an effective system temperature to be around 73 K while -10 dB return loss of feeds results in an effective system temperature to be around 55 K. This difference in effective system temperature, ~ 20 K, is substantial compared to the original 50 K system temperature. On the other hand, even with a perfect match between feed and LNA, effective system temperature can only be reduced further by 5 K. Therefore, -10 dB return loss is decided to be the minimum requirement of the CHIME feed.

2.1 The Four Square Antenna as the First Candidate for the CHIME Feed

We have copied the Four Square Antenna (4sq) [9–12] tuned for Molonglo Observatory Synthesis Telescope (MOST) [13, 14] because the 4sq comes close on so many of our antenna requirements. The 4sq has the advantage of dual polarization, low cost, high repeatability, wide beam pattern across a wide range, high polarization purity and relatively wide bandwidth, which is around 2:1 at -5dB RL level after being scaled to the CHIME band.

Structure of the 4sq is shown in Fig. 2.1. It consists of 6 printed circuit boards (PCB), which are 1 baseboard with 2 SMAs, 4 stem boards with four microstrip transmission lines and 1 radiating petal board. The baseboard and stem boards together are the baluns to transform unbalanced signal at SMA port to balanced currents in the radiating petal board

2.1. The Four Square Antenna as the First Candidate for the CHIME Feed

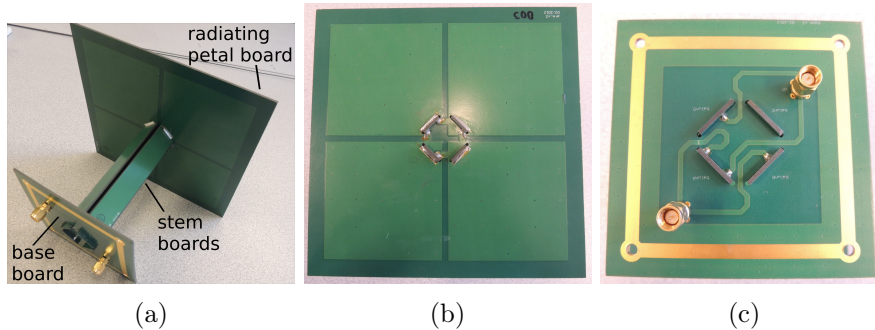


Figure 2.1: (a) Perspective view of the 4sq. (b) Top view of the 4sq, which shows the radiating petal board. (c) Bottom view of the 4sq, which shows the baseboard with 2 SMA and each of them connects 2 microstrip traces. All these four traces continue to four microstrip transmission lines along the four stem boards.

2.1.1 Working Principles of the 4sq

Dual-polarization response of the 4sq is achieved through a feeding technique called the in-pair feeding.

The easiest way to understand the in-pair feeding is to view the 4sq in transmitting mode. For one polarization, excitation signal is fed to one SMA. The signal is split into two to follow two curved transmission lines on the base board, each of which leads to a transmission line on one of the stem boards. These two split signals are carried along these two stem boards until they reach two of the four ports at the petal board. Each port feeds a pair of adjacent petals, as shown in the left of Fig. 2.2, where the red shielded sections are defined as a port. It can be seen that there are four ports in total. The two ports which are excited under this polarization are not adjacent to each other. Therefore all four petals are involved as two parallel pairs.

The right of Fig. 2.2 illustrates how balanced currents on petal A and petal D are transformed from unbalanced signal on stem A. Microstrip stem boards are represented by coax cables for easier illustration. To be more specific, bottom layer of a stem board, which is grounded, is represented by a coax's metal shielding and top layer of a stem board, which is the microstrip trace, is represented by the center conductor of a coax. We can see that by introducing an extra connection between petal D and bottom layer of stem D, currents on the pair of petals are balanced. This extra connection maps to the gray shielded section in the left.

2.1. *The Four Square Antenna as the First Candidate for the CHIME Feed*

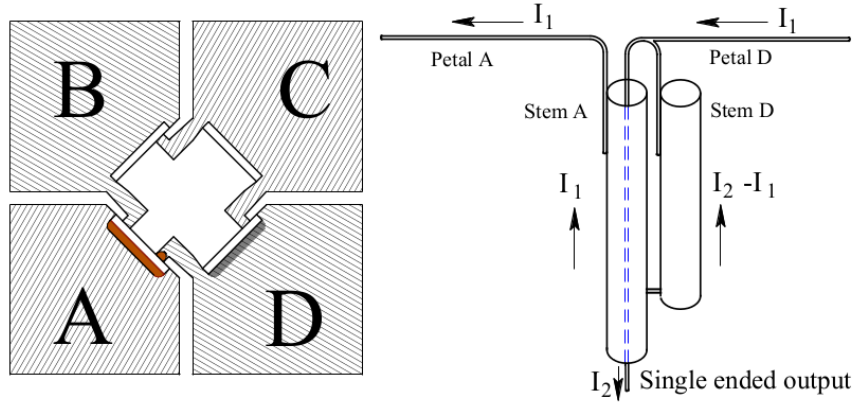


Figure 2.2: Compared with the real petal board in Fig. 2.1 (b), the left is a diagram of 4sq's petal board which exaggerates the center part to illustrate how transmission lines' leads on stem boards connect to petals. The four petals are named respectively as A, B, C and D. The four empty slots are used for insertion of the four stem boards. Stem boards are named A, B, C and D the same order as petals. The red parts is defined as a port. There are four ports in total on 4sq's petal board. The right part of this figure shows how currents on petal A and petal D are balanced from unbalanced signals on stem A by introducing an extra connection between petal D and bottom layer of stem D. This extra connection maps to the gray shielded section in the left.

Similarly, for the other polarization, excitation signal is fed to the other SMA, which is split into two signals following the other two transmission lines and feed petal board at the other two ports. All four petals then work as two parallel pairs of petals whose pattern is perpendicular to that of the previous polarization. A simplified figure to illustrate the general idea of in-pair feeding is shown in Fig. 2.3.

2.1. The Four Square Antenna as the First Candidate for the CHIME Feed

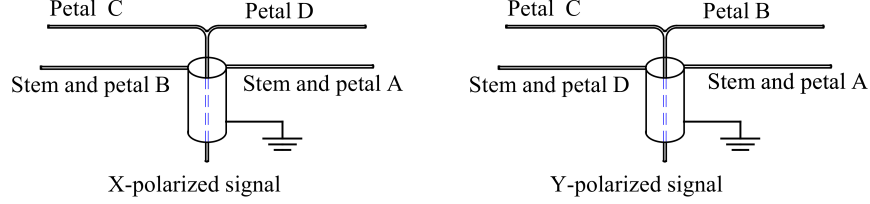


Figure 2.3: This figure shows the general picture of in pair feeding for both polarizations of the 4sq. The naming convention for petals and stem boards is the same as Fig. 2.2. The details on transmission lines along the base board and stem boards are excluded, so it is not a circuit diagram.

The 4sq’s wide bandwidth can be achieved because baluns are microstrip transmission lines, which have great flexibility to transform impedance from the petal board port to standard 50 Ohm at SMA.

2.1.2 CHIME 4sq on the Two Dish System

A set of 4sq, scaled to the CHIME band, were deployed on the two dish system, which is a two-element interferometer located at DRAO as the simplest interferometer prototype of CHIME.

Through the measurements with this two-dish system, we have decided to use low-loss Teflon as substrate of baluns in the future because lossy dielectrics in the balun substrate increases the system temperature.

Petal boards of the MOST 4sq are double-layer and viaed to reduce material loss. To test the effectiveness of this strategy, noise temperatures of two CHIME 4sq have been estimated with the two dish system. These two feeds are exactly the same with viaed double-layer petal boards, except one of them has FR4 based petal board while the other has Teflon based petal board. Fig. 2.4 (a) shows the rough estimation of their noise temperature. The similar noise temperature of these two feeds proves that lossy dielectric material in the petal board does not increase system temperature because of vias. Therefore, in the future, petal board would be double-layer and viaed, with lossy but cheap FR4 as the substrate.

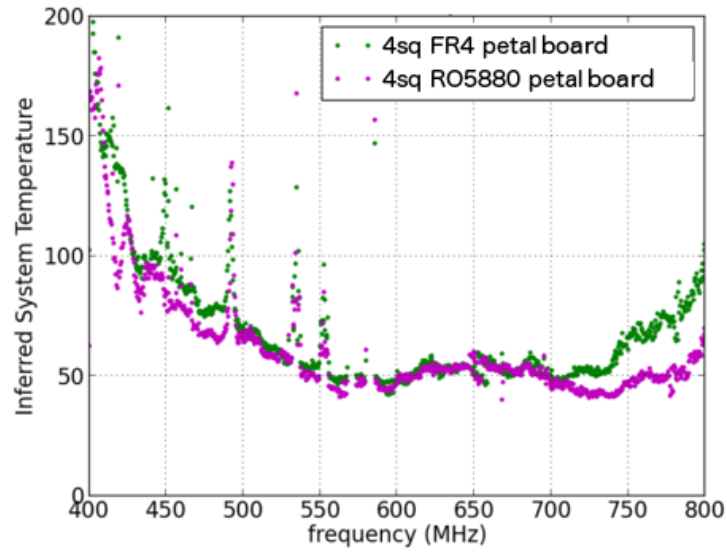
We have found the two-dish system with the 4sq feed is noisier than the tolerable level, mainly due to 4sq’s impedance mismatch to LNA. Return loss measurement of the CHIME 4sq is shown in Fig. 2.4 (b). It can be seen that: firstly, return loss is smaller than -5dB rather than required -10 dB in a 2:1 bandwidth; secondly, that band is higher than CHIME’s desired band.

2.1. *The Four Square Antenna as the First Candidate for the CHIME Feed*

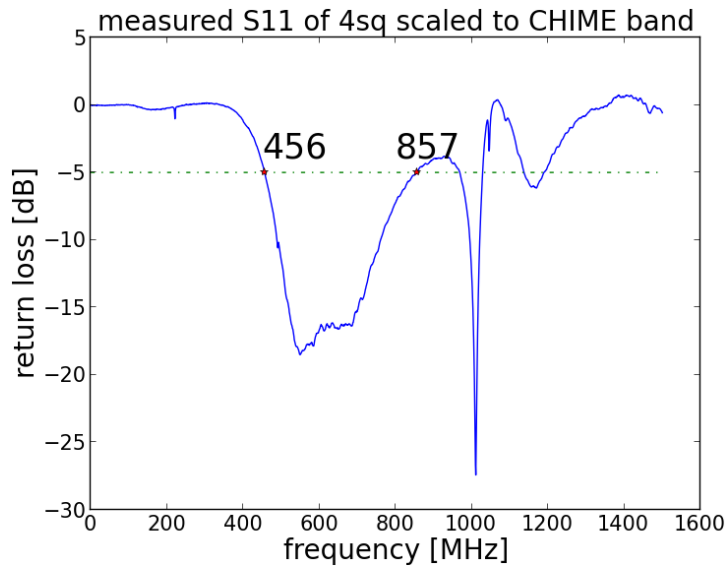
Impedance match between feed and LNA is a key aspect that is improved in this thesis.

In the manufacture point of view, the 4sq is robust enough to last several winters unprotected.

2.1. *The Four Square Antenna as the First Candidate for the CHIME Feed*



(a)

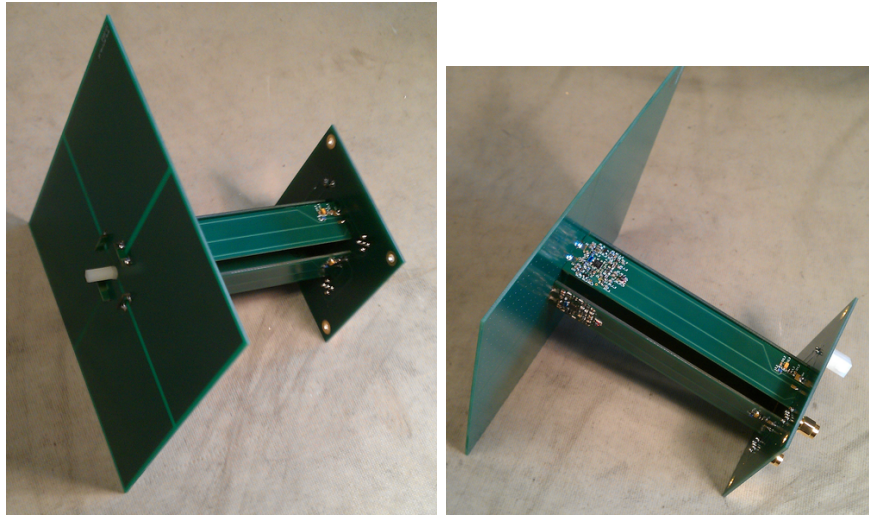


(b)

Figure 2.4: (a) Rough estimation of noise temperature of 2 4sq feeds. One of them has FR4 based petal board while the other one has Teflon based petal board. (b) Return loss measurement of the CHIME 4sq.

2.2 The Active 4sq

Rather than having LNA to be an independent element in the analog chain, LNA can be incorporated to feed, by designing a low noise amplifier circuit to feed the 4sq's petals directly without introducing baluns. This is called an active feed. We explore this option to eliminate the baluns and thus the loss in the baluns. An active 4sq has been designed and built by Gregory Davis, as shown in Fig. 2.5. Fig. 2.6 shows the measurement of its beam pattern by Keith Vanderlinde. It can be seen that the beam patterns are not smooth and there is non-negligible asymmetry in the co-polar beams because the LNA circuit does not balance petal currents well. Therefore, this kind of active feed is rejected.



(a) Perspective view of the active 4sq (b) Side view of the active 4sq

Figure 2.5

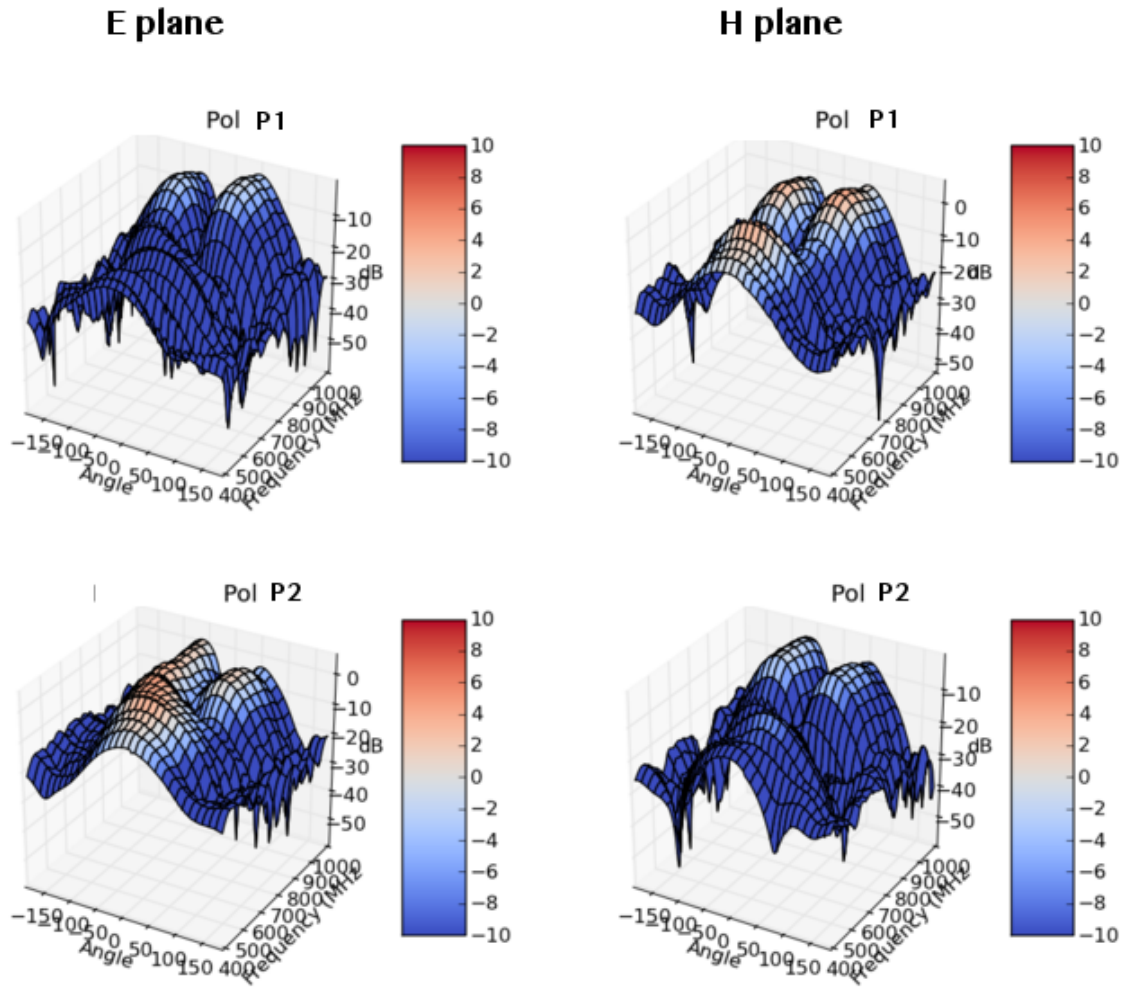


Figure 2.6: Active 4sq's beam measured by Keith Vanderlinde in the University of Toronto. Pol P2 is the polarization parallel to E plane, ie, xz plane. Pol P1 is the polarization parallel to H plane, ie, yz plane.

2.3 The Four Point feed and The Four Sleeve feed

The 4sq feed has the problem of impedance mismatch to LNA, so two modifications of 4sq have been tried, which are the four point feed (4pt) and the four sleeve feed (4sl). They are also based on in-pair feeding technique.

Fig. 2.7 (a) shows a picture of the 4pt and Fig. 2.7 (b) shows the measured return loss of this 4pt. It can be seen that bandwidth of the 4pt is still far away from CHIME's requirements.

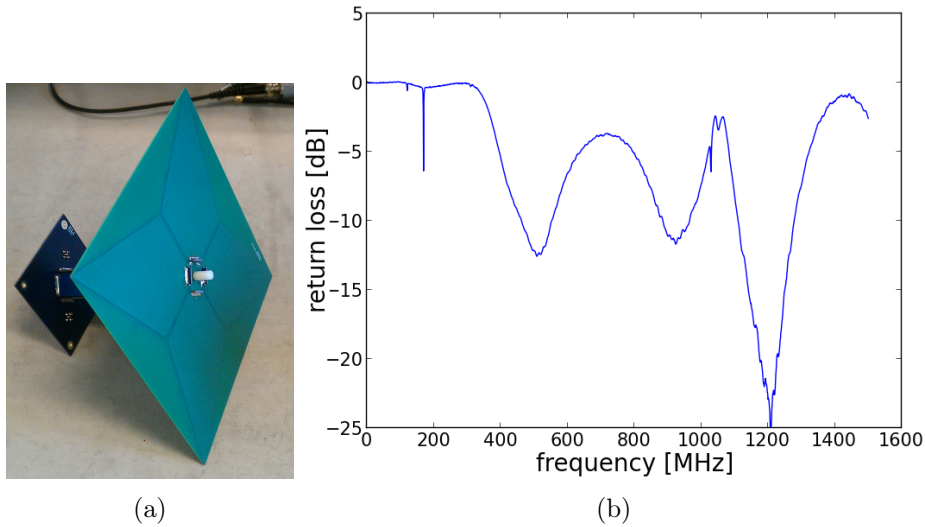


Figure 2.7: (a) A picture of the 4pt built as a modification of the 4sq. (b) Measured return loss of the 4pt.

Fig. 2.8 (a) shows a picture of the 4sl. Each petal looks like a sleeve. There are two extra disks added on top of the petal board. They are used to tune the impedance. Fig. 2.8 (b) shows the measured return loss of this 4sl with tuning of the two disks. It can be seen that bandwidth of the 4sl is pretty satisfying. However, its petal size is too big to be azimuthally rotated in the CHIME feed array. Azimuth rotation of feed in CHIME array enables the ability to do more tests. Moreover, disks above the petals are floppy and do not survive field environment. Removing floppy disks makes the impedance match of the 4sl no better than the 4sq or the 4pt.

2.3. The Four Point feed and The Four Sleeve feed

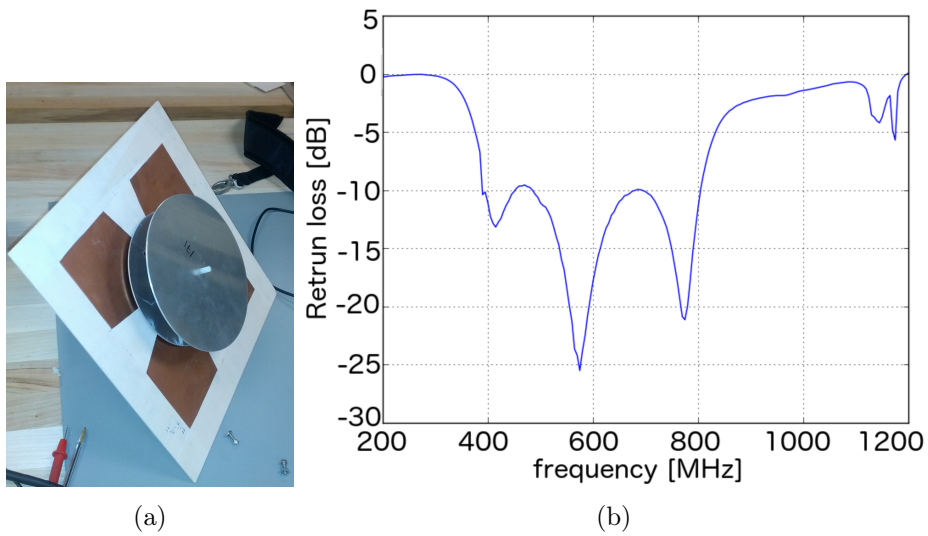


Figure 2.8: (a) A picture of the 4sl built as a modification of the 4sq. (b) Measured return loss of the 4sl.

These two trials, along with some other modifications, are not satisfying to be used as CHIME feed. Therefore, a new feed needs to be designed.

Chapter 3

Method

To design a wide bandwidth feed for CHIME, the loop is: begin with designing a feed; then simulate it with CST; after simulation, the designed feed is built and measured; measured results are compared to simulated results to verify the simulation; disagreement between measurement and simulation leads to re-simulation of the design until they agree; if agreement between measurement and simulation is achieved, a new design is formed based on performance of the previous design, previous steps are looped until all CHIME's feed requirements are satisfied by a particular design.

Feed itself can be simulated by Computer Simulation Technology (CST) ³ to get its current pattern, beam pattern and impedance spectra. Among them, beam pattern can be measured in the anechoic chamber in University of Toronto, impedance spectra can be measured by Vector Network Analyzer (VNA) in the UBC lab.

Feed installed on focal line can be simulated by Grasp ⁴ to get the sky beam, which is a reflection of feed illumination on the cylindrical reflector. A slice through the far-field beam of the telescope can be measured by observing the signal as a pulsar or bright source transits, and these measurements are compared to models.

3.1 Grasp

GRASP is a commercial software package which simulates optical beams by applying the physical theory of diffraction (PTD) and physical optics (PO) to calculate currents when a transmitting antenna illuminates a reflector.

The basic simulation procedure is:

1. a user sets up geometry of feed and reflector;
2. surface of reflector is meshed automatically by Grasp;

³<https://www.cst.com/>

⁴<http://www.ticra.com/products/software/grasp>

3.1. Grasp

3. the user imports the beam pattern of feed from CST simulation as illumination to reflector;
4. E field and B field are calculated by Grasp at each mesh grid on the reflector's surface according to the feed illumination pattern;
5. induced current on each mesh grid is calculated through PO or PTD from field distribution on reflector's surface; and
6. field radiated from the current distribution in step 5 is calculated and added to the original field.

CHIME's beam to the sky is the far-field limitation of step 6. As an example, Fig. 3.1 visualizes the above procedure. If there are additional structures involved to make the system have multi-reflection path, step 4-5-6 would be looped to include the additional reflections.

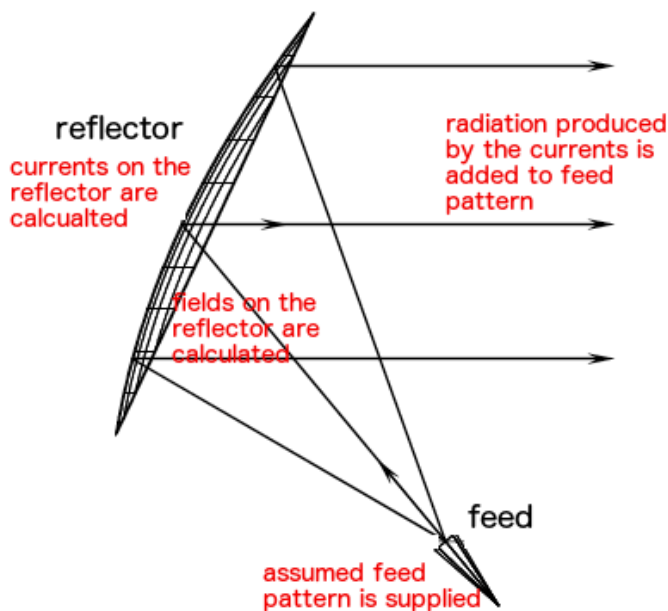


Figure 3.1: An offset circular dish together with a feed at its focus with one reflection path considered to illustrate Grasp simulation procedure.

Grasp will be used to simulate interaction between feed and reflector to get beam on the sky after feed has been designed by CST.

3.2 CST

CST has different solvers for electromagnetic analysis under different cases. The one used in CHIME feed design is transient solver⁵. The basic principle of transient solver is Finite-Difference Time-Domain (FDTD) [15], which solves Maxwell equation in 3D spatial grid step by step in the time domain.

3.2.1 CST Simulation Overview

A CST user must construct a three dimensional model of an antenna and make several operational choices, particularly about the desired accuracy of results, the distance scale of physical interpolation (the mesh scale for calculations), the size and shape of the volume to be simulated and the frequency range of interest.

CST treats the antenna under study as a transmitter, which is simply time-reversed from our intended use, and calculates a beam pattern using the following steps.

1. Generates a closed box whose walls are a few perfect matching layers (PML) to encompass the antenna totally but do not touch it.
2. Meshes the entire space, which is closed by PML, according to antenna's material properties and dimensions.
3. Feeds an excitation signal in time domain to antenna's input port, such as SMA port.
4. Starts updating E field, B field, current and charge at all mesh grids once a time by following the FDTD algorithm.
5. Calculates and stores total energy in the closed box at each time step and stops calculation if total energy is smaller than some user specified value.

The physical picture of step 4 is: the excitation signal, started from the input port, propagates along the mesh grids as time goes; signals propagate in space until they reach PML layers and get absorbed because of special Electromagnetic properties of PML, just like in open space without any reflection back to structure.

In the post process, signals in time domain at the input port are stored and go through FFT to get input impedance in the frequency domain. E

⁵<https://www.cst.com/Products/CSTmws/TransientSolver>

field in time domain on the inner surface of PML are stored and go through FFT to get signal in frequency domain. Then for each frequency channel, E field on PML's inner surface is integrated and transformed to get far-field beam pattern. E field or B field or current at any mesh knot in the closed space can be stored for other usage, for example, to get material loss and to view current distribution.

3.2.2 Test of our Approach to CST through A Dipole Model

The validity of our approach to CST simulation is checked through dipole, which is the simplest and most widely used antenna. The basics of dipole is two identical conductive elements, such as two rods, fed in the middle by transmission line, as shown in Fig. 3.2 (a). What we are interested is the half-wavelength dipole whose total length is half of the working frequency's wavelength, ie, $L = \lambda/2$.

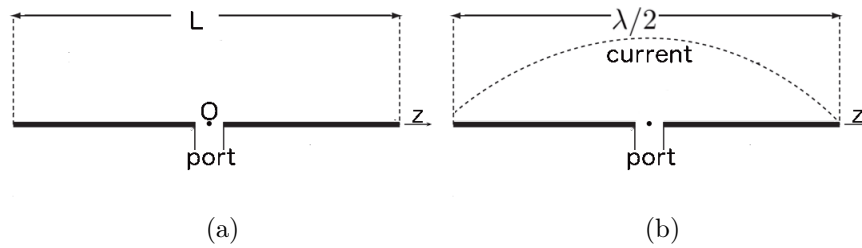


Figure 3.2: (a) A typical dipole with two conductive elements whose total length is L . For convenience, origin of the coordinate system is set at the center of dipole, and the z-axis is along the dipole. (b) Current distribution in sine form. Image source: http://electronicdesign.com/site-files/electronicdesign.com/files/uploads/2013/07/0613WTDantennas_FIG2.gif.

The performance of dipole is well measured, widely accepted and can be worked out analytically under ideal assumptions or numerically through Methods of Moments (MoM) using Python or numerically through FDTD, which is realized by CST simulation.

All these three approaches to work out the performance of the dipole are carried out and compared to each other to validate our understanding of CST.

Analytical Calculation

In the ideal case, the rods are infinitely small, there is only current parallel to z-axis. The gap between the rods is also infinitely small so that it does not affect current distribution. At the end of each rod, the current is zero since there is just no where for the current to go. At each single frequency, the current distribution should be a sine function, as shown in Fig. 3.2 (b) and Eq. 3.1:

$$I(z) = \begin{cases} I_0 \sin[k(\frac{l}{2} - z)], & 0 \leq z \leq \frac{l}{2} \\ I_0 \sin[k(\frac{l}{2} + z)], & -\frac{l}{2} \leq z < 0, \end{cases} \quad (3.1)$$

where k is the wave number defined by $k \equiv \frac{2\pi}{\lambda}$.

Since current distribution is already known under ideal case assumption, the next important parameter of an antenna would be its input impedance. Real part of input impedance is calculated first for simplification. The idea to calculate real input impedance is that: real input impedance represents power radiated off by the antenna through the input port. Since $P = I(t) \times V(t)$, power has a non-zero average if the ratio V/I is real. Power has a zero average if the ratio V/I is imaginary therefore imaginary input impedance represents power stored near antenna:

$$P_{rad} = \frac{|I_{in}|^2}{2} R_{in}, \quad (3.2)$$

where P_{rad} is radiated power, I_{in} is current at input port and R_{in} is real part of input impedance.

To calculate the real part of input impedance, first calculate far field according to current distribution, as:

$$E_{\theta} \simeq j\eta \frac{I_0 e^{-jkr}}{2\pi r} \left[\frac{\cos(\frac{\pi}{2} \cos\theta)}{\sin\theta} \right] \quad (3.3)$$

$$H_{\phi} \simeq j \frac{I_0 e^{-jkr}}{2\pi r} \left[\frac{\cos(\frac{\pi}{2} \cos\theta)}{\sin\theta} \right], \quad (3.4)$$

where η is the intrinsic impedance of the vacuum, defined as $\eta \equiv \sqrt{\frac{\mu_0}{\epsilon_0}} \simeq 377$ (Ohm).

As a result, the power in the farfield is

$$P_{rad} = \oint \frac{1}{2} \text{Re}[E \times H^*] ds = \eta \frac{I_0^2}{4\pi} \int_0^{\pi} \frac{\cos^2(\frac{\pi}{2} \cos\theta)}{\sin\theta} d\theta = \eta \frac{|I_0|^2}{8\pi} C_{in}(2\pi), \quad (3.5)$$

where $C_{in}(x) = 0.5772 + \ln(x) - \int \frac{\cos(y)}{y} dy$.

Therefore, the real part of input impedance R_{in} is

$$R_{in} = 2 \times \frac{P_{rad}}{I_0^2} \simeq 73 \text{ (Ohm)}. \quad (3.6)$$

Similarly, to get the imaginary part of input impedance, near field is calculated from current distribution and then integrated along the surface of dipole, as shown in Chapter 8 of [16]. The full input impedance for an ideal dipole is

$$Z_{in} = 73 + 42.5j \text{ (Ohm)}. \quad (3.7)$$

MoM Numerical Calculation

Method of moments (MoM) is generally believed to be a reliable numerical method to analyze EM problems, but sometimes it can be very time consuming. To apply MoM method to dipole, the basic assumption is that current on the rods of dipole has only z-component and has no variation on the rods' circumference. Therefore current on the rod surface can be presented by current in the rod center with equal magnitude.

The steps to deploy MoM is:

1. apply a voltage V_{in} to the gap between the two rods;
2. with the distance d between the two rods, calculates the E field in the gap simply as $E_{gap} = \frac{V_{in}}{d}$;
3. divide these two rods into small pieces, say N pieces, so that each piece of rod has the length $l = \frac{L}{N}$. Assume each piece i has its own current I_i constantly distributed along its length;
4. calculate the field along the surface of rod generated by these pieces of currents. Field is a function of these currents $[I_0, I_1, \dots]$;
5. work out the solution of $[I_0, I_1, \dots]$ so that E field generated by these currents cancels the original E field generated by V_{in} (As a result, current distribution along the rod is achieved, together with the input port current I_{in} .); and
6. with V_{in} and I_{in} calculates the input impedance Z_{in} simply as $Z_{in} = \frac{V_{in}}{I_{in}}$.

The finer the rod is divided, the more accurate the result is. There are some other small techniques can be applied, such as: current on each small piece can be in parabolic or triangular form rather than constant form to improve the smoothness of currents along the whole dipole. Also, symmetry of dipole can be used to simplify calculation. With this in mind, python scripts have been written to calculate current distribution and input impedance of a half-wavelength dipole.

CST Calculation

As mentioned before, to use CST to calculate properties of dipole antenna, a model needs to be set up first, as shown in Fig. 3.3.

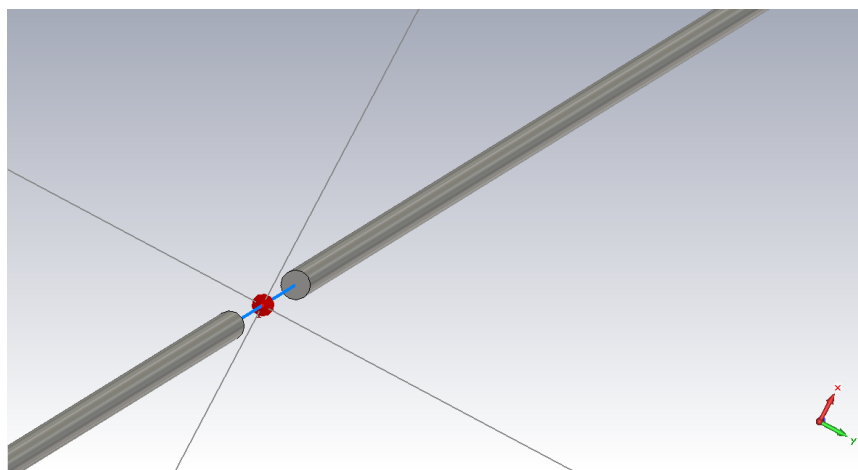


Figure 3.3: A dipole model set up in CST. The two gray rods are the perfect electrical conductor (PEC) and they are separated by a gap to place an excitation discrete port⁶, which is the red cone.

The parameters to describe this dipole and CST settings are:

rN : $\frac{2L}{rN}$ defines the radius of rod. the bigger the rN , the smaller the rod

gN : $\frac{L}{gN}$ defines the gap between the two rods. The bigger gN , the smaller the gap

$lpwv$: number of mesh per wavelength, defines the general mesh density

dx : number of mesh lines across the radius of the rod cross section, defines the local mesh density

$bodwv$: wavelength/ $bodwv$ is the nearest distance between PML and dipole antenna

Other parameters can also be manipulated but results are not sensitive to them, so they are not listed here. In the CST simulation, the bigger the $lpwv$ and dx , the more accurate the result should be. A very important tip is that:

no matter what is the object that needs to be analyzed, make sure the simulated result is converged if only CST simulation parameters are refined because there is only one true fact of the object which does not depend on how it is simulated.

Therefore, during the CST simulation procedure, I have refined $lpwv$, dx , $bodwv$ step by step until the input impedance is converged within 1.5% for each set of $[rN, gN]$.

Comparison among Analytical Solution, Python MoM and CST FDTD

After current distribution and input impedance of dipoles have been obtained through these three methods, these results are compared to check our approach to CST simulation.

Fig. 3.4 shows the three components of dipole's currents simulated by CST. It agrees with the analytical assumption and MoM assumption that, currents are mainly aligned along the z-axis. Z-component of currents calculated from different methods are compared in Fig. 3.5. It is shown that they generally agree with each other, the small difference between CST and analytical calculation is caused by the finite gap and finite radius of rod in the CST model, while the analytical calculation is assuming an ideal case. It is not clear here to say which result is more accurate, but it definitely confirms that CST simulation here repeats classic idea. Confirmation of CST's ability to simulate current is also a confirmation of CST's ability to simulate antenna's beam pattern.

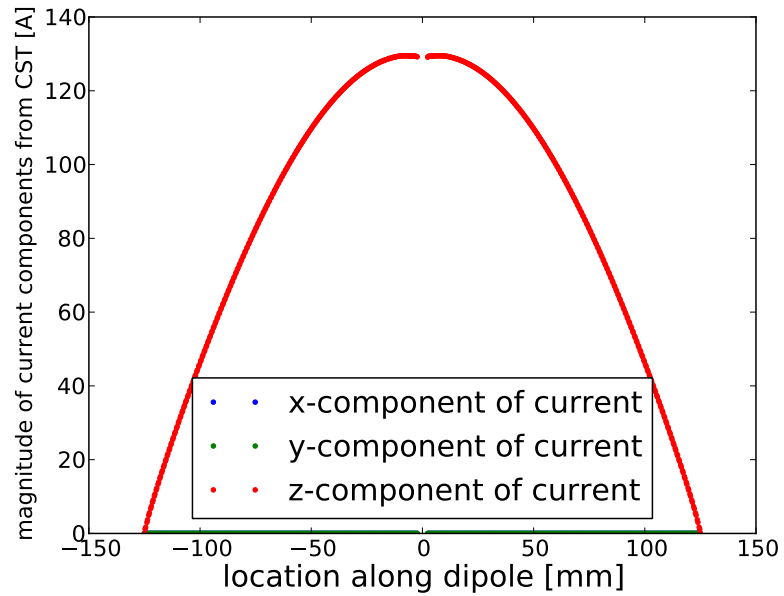


Figure 3.4: Three components of dipole's currents simulated by CST. The half-wavelength dipole's frequency is centered at 600 MHz, so its length is 250 mm. X-component and Y-component are almost zero, which repeats the classic picture that currents on dipole mainly align with the rods.

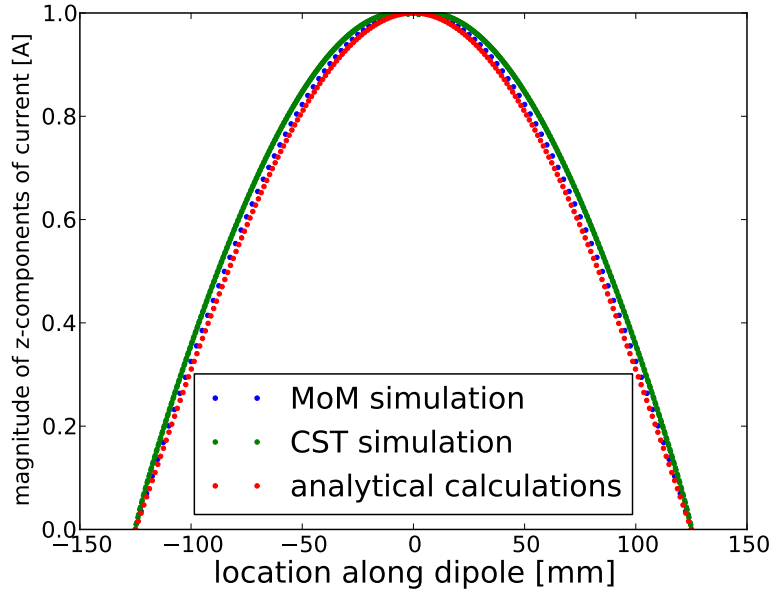


Figure 3.5: Z-components of current distribution given by MoM simulation CST simulation and analytical calculation are compared. The good agreement among them validates my approach to CST to understand dipole's current pattern.

Another important parameter of antenna is input impedance and its comparison among these three approaches is shown in table 3.1. As rN gets bigger, the value given by CST is closer to analytical value, and it should be. When rN gets bigger than 10100, CST is not able to simulate because the very small structure requires very small mesh, thus too much memory is needed. For finite value of rN , the different impedances given by CST and MoM imply 1 % difference in reflected power, which is already the best that CST can do. I find this level of agreement is good enough to support my approach to CST considering that MoM has simplified assumptions too.

The agreement on both current distribution and input impedance among CST simulation, MoM method and analytical solution under ideal assumption confirms the validity of CST and my understanding of it. Therefore, CST would be used in the future analysis and design.

3.2. CST

Table 3.1: Input impedance comparison for half-wavelength dipole for different values of rN , while fixing $gN=100$.

| rN | 1000 | 5000 | 10000 | 10100 | 20000 | ∞ (theory) |
|--------------------------|-----------|-----------|-----------|------------|-----------|-------------------|
| CST (real, imaginary) | (86,54.1) | (82,50.8) | (80,47.5) | (79, 48.9) | N/A | (73,42.5) |
| MoM (real, imaginary) | (83,44.3) | (76,42.4) | (75,42.0) | (75,42.0) | (74,41.8) | (73,42.5) |

3.2.3 Plan of Use

To design a CHIME feed, following plans to use CST are made.

1. CST Model of 4sq and its variants would be constructed to get their current distributions so that our physical understanding of these feeds would be improved. Beam pattern would be modeled at the same time and compared to measurement so that validity of models can be checked.
2. The 4sq would be modeled by CST through various efforts until simulated impedance spectra agree with measurement. The ability to simulate impedance spectra accurately is mandatory before applying CST to design wide bandwidth feed.
3. The believable simulation technique gained from step 2 would be used to test different ideas of designing until a promising design is found.
4. The same technique would be applied again to optimize the design found in step 3 until CHIME's specific requirements are satisfied.

Chapter 4

Modeling the Current Patterns, Beam Shapes and Impedance Spectra of Single Feed 4sq and its Variants

Modeling is to help improve understanding 4sq and its variants so we can get some intuition on how to design a new feed. In addition, the ability to model impedance spectra is mandatory to design a new wide band feed.

4.1 Visualizing Current Patterns and Beam Shapes

CST has been used to predict the current pattern and the radiative properties of a 4sq antenna, a 4pt and a 4sl.

4.1.1 The 4sq and Its Petal board Model

A simplified 4sq petal board model has been built in CST to represent the real 4sq, as shown in Fig. 4.1 (a). Fig. 4.1 (b) shows the front view of the model. Frequency range of this model is set to 400 MHz to 800 MHz.

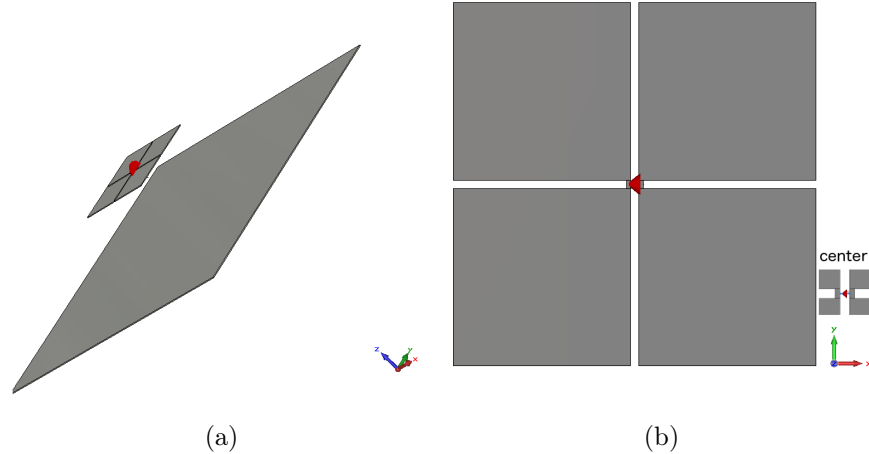


Figure 4.1: (a) Petal board model of the 4sq. Petal board and ground plane are present but stem boards and baseboard are not included because they are measured to have almost no influence on the beam pattern. Ground plane is just present in space rather than electrically connected to the 4sq antenna. (b) Front view of the 4sq petal board model. Since balun’s usage is to balance current on the petal board, so the complex, detailed feeding traces on real petal board are replaced with a symmetric discrete port, as shown in the lower right corner. The coordinate system is set that feed is pointing up to the positive z-axis, and feed is excited in the polarization parallel to the x-axis.

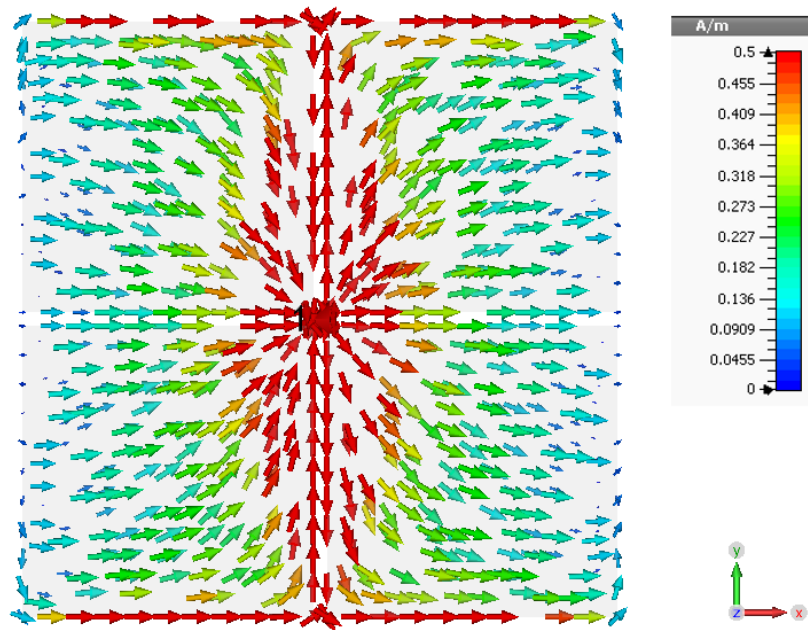
Current Pattern

To understand radiating mechanism of the 4sq, current patterns at different frequencies are needed. Left of Fig. 4.2 shows the current distribution on petal board at a phase ⁷ at 600 MHz ⁸. At each frequency, current at each spatial point just varies sinusoidally in time, so it is informative enough to look at absolute magnitude distribution of the current, as shown in the right of Fig. 4.2.

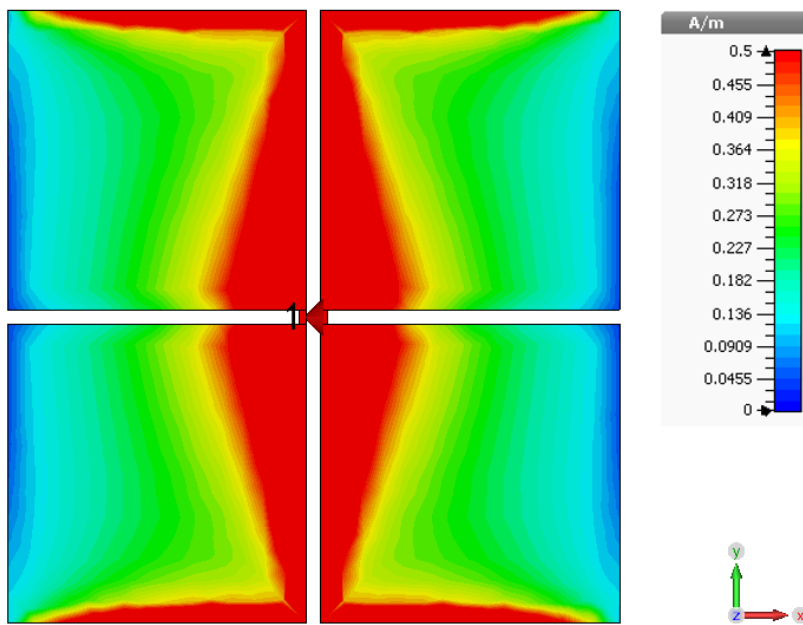
⁷“at a phase” means at a point in the time domain.

⁸600 MHz is chosen for representation of a wide band antenna because 600 MHz is the center frequency of our frequency range and 4sq’s radiating property smoothly varies in frequency.

4.1. Visualizing Current Patterns and Beam Shapes



(a) Current distribution at a phase at 600 MHz



(b) Absolute magnitude distribution of current at 600 MHz

Figure 4.2: Current pattern of a 4sq which shows that currents concentrate on edges of the petals.

It is shown that when the petal board is fed with x-polarized excitation signal, currents on the y-axis-aligned inner petal edges are opposite in direction, so they attract each other. Currents on the x-axis-aligned inner petal edges are in the same direction, so they repel each other. Finally, currents condense along the y-axis-aligned inner edges and the x-axis-aligned outer edges. Moreover, since currents along the two pairs of inner edges are in opposite direction, they cancel each other and do not contribute to radiation. Currents on these four x-axis-aligned outer edges are all in the same direction at any time and these currents form the basis of 4sq's radiation pattern. Therefore, for each polarization, the basics of the 4sq is a pair of face-to-face bent dipoles, fed by a common input, as shown in Fig. 4.3.

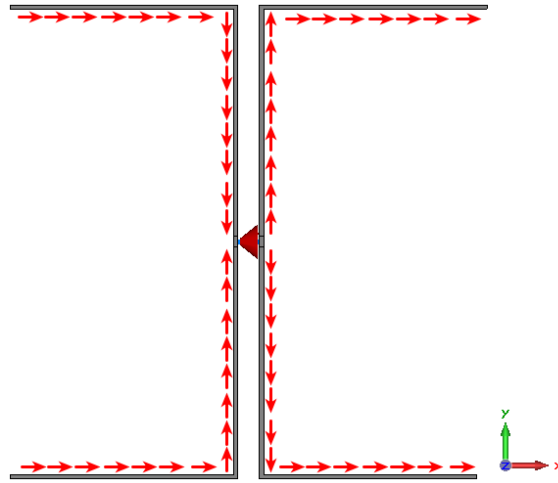


Figure 4.3: T dipole model representing the basics of current distribution on the 4sq. Gray parts are the metal to represent structure of T dipoles. Red arrows indicate the path and direction of currents excited by the port.

Current patterns at other frequencies show the same idea, except that ratio of currents' magnitude along inner edges to currents' magnitude along outer edges changes with frequency.

Beam Pattern

Keith Vanderlinde has measured the H plane of the 4sq, which can be used to check whether the previous 4sq petal board model is correct or not. If it is correct, simulation of the petal board model can give us information on E

4.1. Visualizing Current Patterns and Beam Shapes

plane, which is not measured.

To begin with a visual idea, Fig. 4.4 shows the 3D presentation of simulated 4sq's beam pattern at 600 MHz. It can be seen that the beam pattern is pretty smooth in the forward direction of the 4sq and there are three side lobes in the backward direction. Note, this beam pattern is for the x polarization. Beam's 2D view is shown in Fig. 4.5. Beam patterns at other frequencies are similar to this one except for small differences in directivity and beam width. E plane's beam width across 400 MHz to 800 MHz is $\sim 60^\circ$, while H plane's beam width across band is $\sim 60^\circ$.

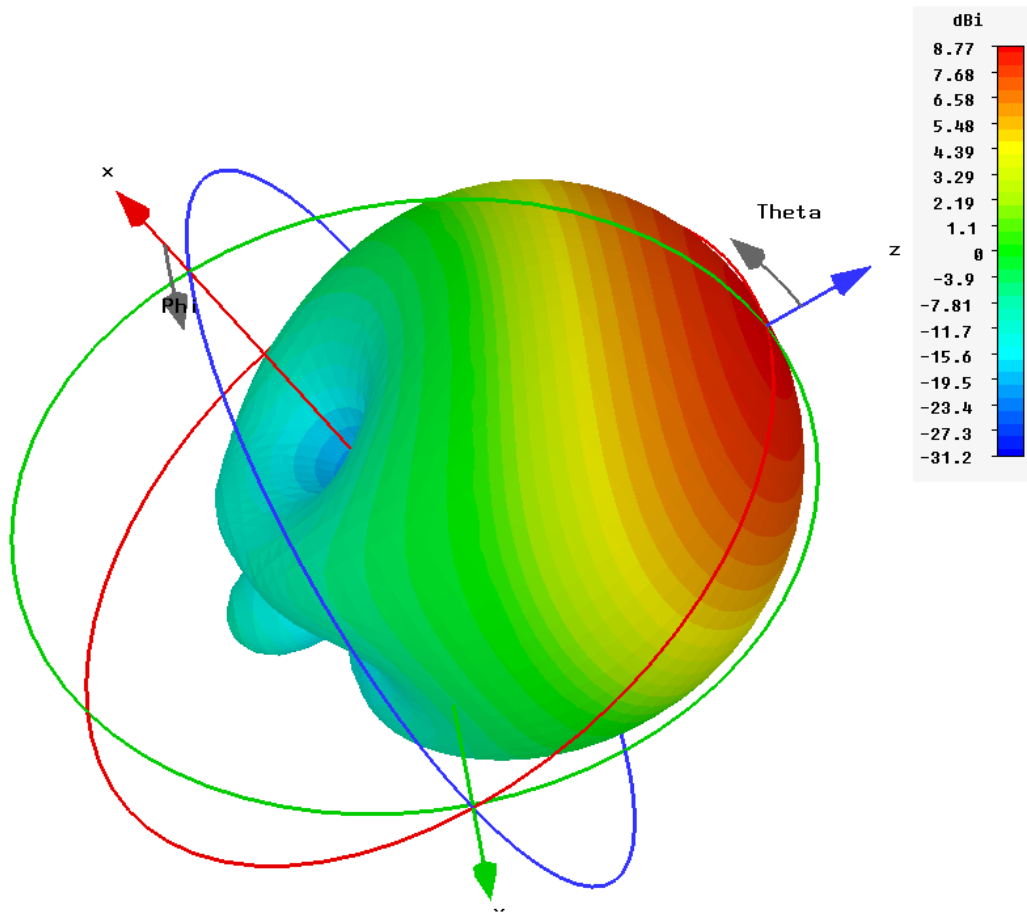
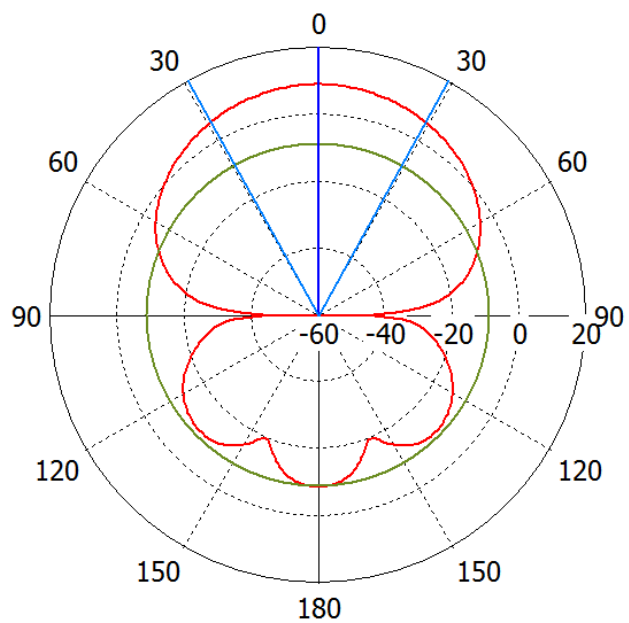
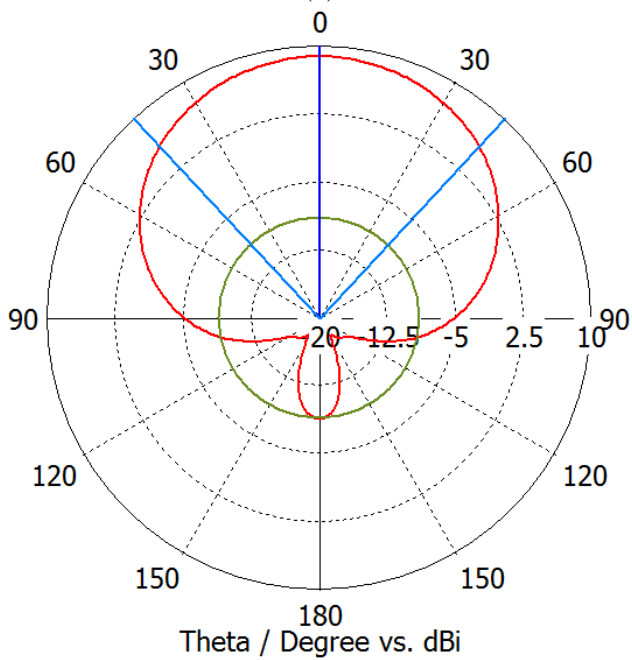


Figure 4.4: 3D representation of simulated 4sq's beam at 600 MHz. The beam is smooth and broad in the forward direction.



(a)



(b)

Figure 4.5: (a) Simulated E plane of 4sq's beam, with beam width to be 58.3° . (b) Simulated H plane of 4sq's beam, with beam width to be 85.8°

4.1. Visualizing Current Patterns and Beam Shapes

To better compare the CST simulation with measurement, beam pattern of the 4sq at several frequencies in CHIME band are simulated and fitted to a Gaussian distribution with centroid and 3dB beam width as fitting parameters. The same fitting is done for the measurement of 4sq's H plane at several frequencies. Beam widths from these two fittings are compared numerically to check CST's validity, as shown in Fig. 4.6. We can see there is a pretty good match between simulation and measurements, confirming our current understanding of current pattern and beam pattern.

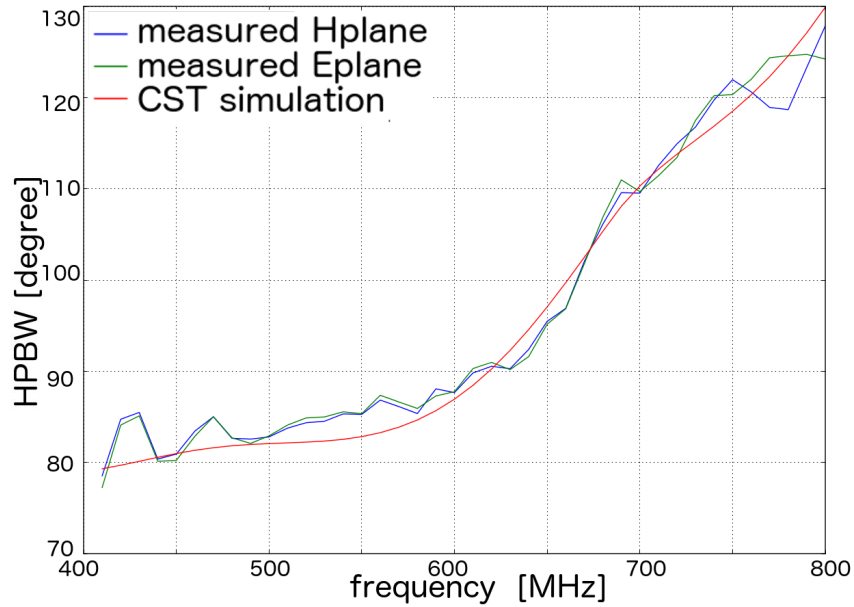


Figure 4.6: The 4sq's H plane beam width comparison between CST simulation and measurements. They agree well with each other, confirming 4sq's simulation and understanding got from simulated results are believable.

Centroids of simulated beams are almost zero because geometry of the 4sq petal board model and all CST settings are symmetric. Zero centroid is a confirmation of CST simulation. Centroids of measured beams have offsets compared to simulations because of practical factors, like asymmetric feeding traces in the center of petal board and the asymmetric geometry of the anechoic chamber where beams are measured, which are not included in CST

model. Therefore, centroids between simulation and measurement should be different. Further more, we should not bother to try to put these details in CST model, because they can be changed in future CHIME feed candidate and does not affect our current purpose to understand 4sq's radiating mechanism.

This centroid disagreement is a very good example that we should understand what is the model and be clear what is the expected difference between model and reality. The truth is that we can never build a model which is exactly the same as the real case.

4.1.2 4sq's Variants and Their Petal Board Models

The 4pt and the 4sl, which have been built and tested already through experimental trials, are modelled to get their current distribution and beam shape. A grasp of the similarity and difference in EM behavior among the 4sq, the 4pt and the 4sl is necessary to decide which path to take in future feed design.

The Four Point Feed

The geometry of 4pt's petal board is shown in Fig. 4.7 (a), whose 600 MHz current distribution at a phase is shown in Fig. 4.7 (b). It can be seen that it basically follows the same radiating mechanism as the 4sq, ie, currents condense along edges of petals. Beam pattern of the 4pt at 600 MHz is simulated, as shown in Fig. 4.8. Compared with beam patterns of the 4sq, 4pt's beams are basically the same. They are smooth and broad in the forward direction.

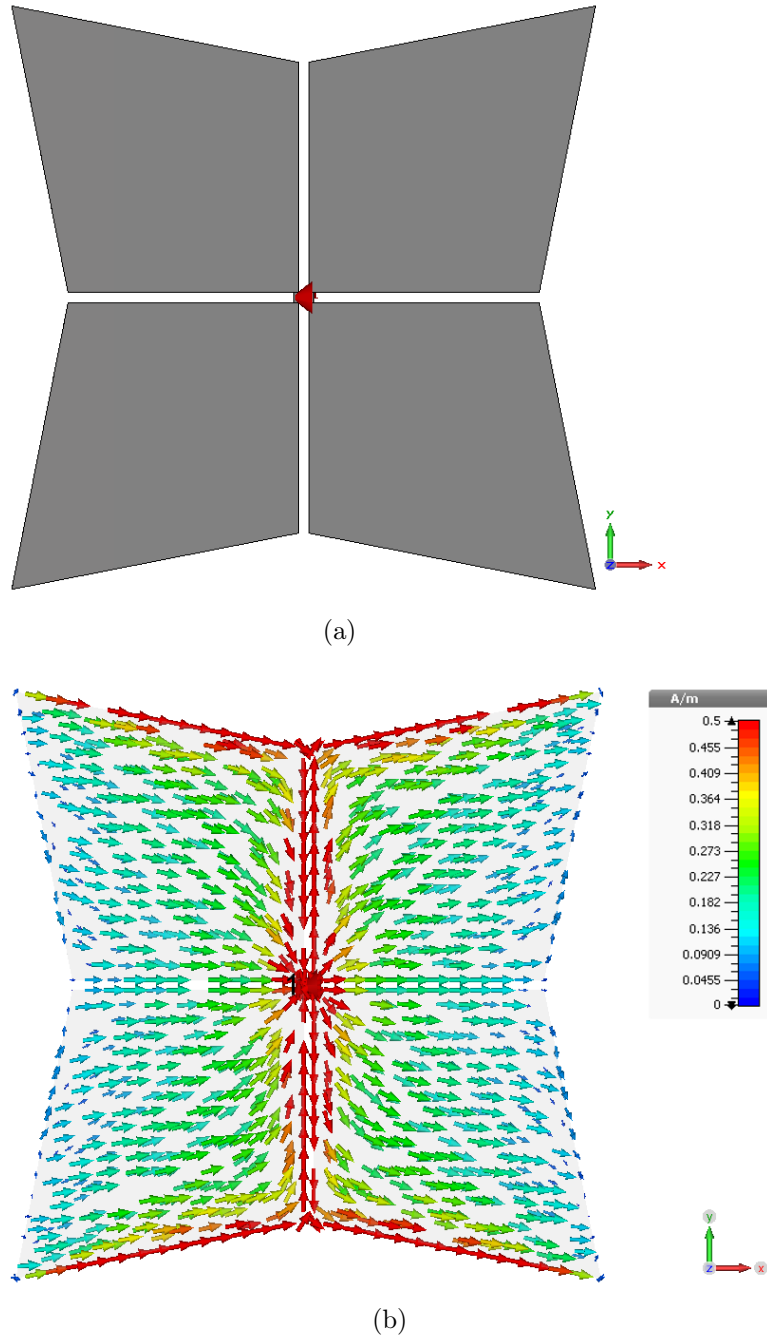


Figure 4.7: (a) Geometry of the 4pt petal board. (b) Current distribution of the 4pt at 600 MHz at a phase. Currents of the 4pt concentrate on edges again like the 4sq.

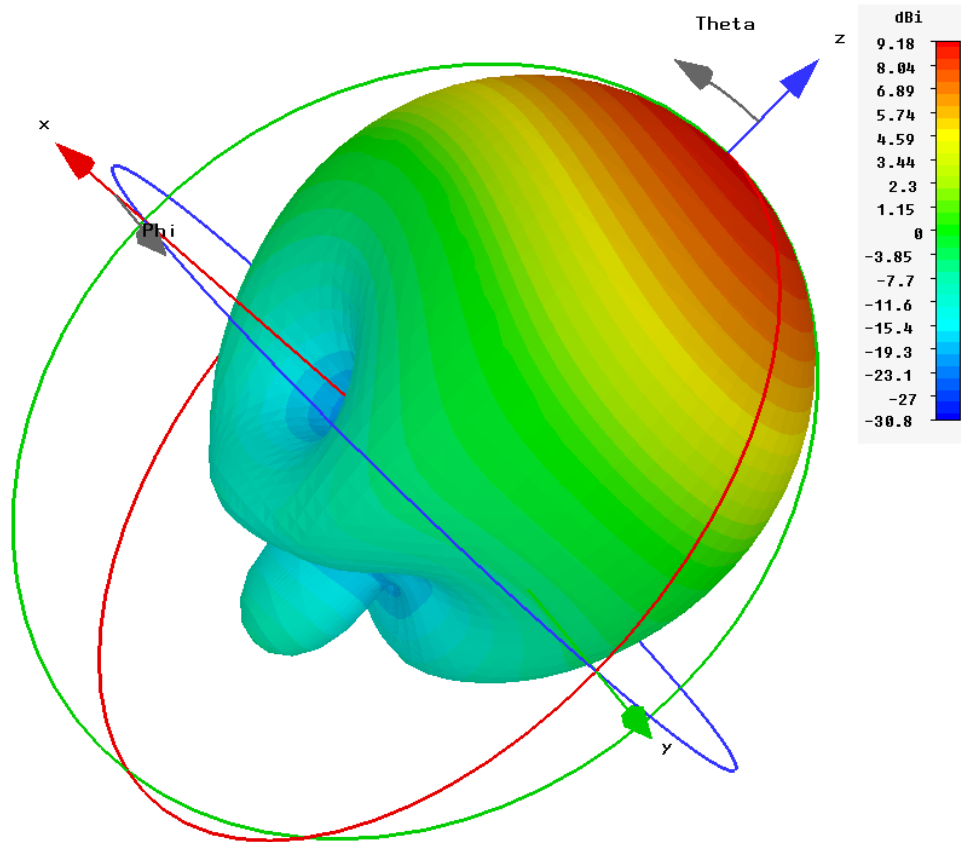


Figure 4.8: 3D representation of 4pt's beam at 600 MHz. E plane's beam width is 55.9° . H plane's beam width is 77.7° .

The Four Sleeve Feed

Another variant which has been simulated is the 4sl without disks. The geometry of the 4sl's petal board is shown in Fig. 4.9 (a), whose 600MHz current distribution at a phase is shown in Fig. 4.9 (b). It can be seen that the 4sl again basically follows the same radiation mechanism as the 4sq and the 4pt. Simulated beam pattern of the 4sl is shown in Fig. 4.10. Compared with beam pattern from the 4sq and the 4pt, the 4sl beam shares the same characteristics.

4.1. Visualizing Current Patterns and Beam Shapes

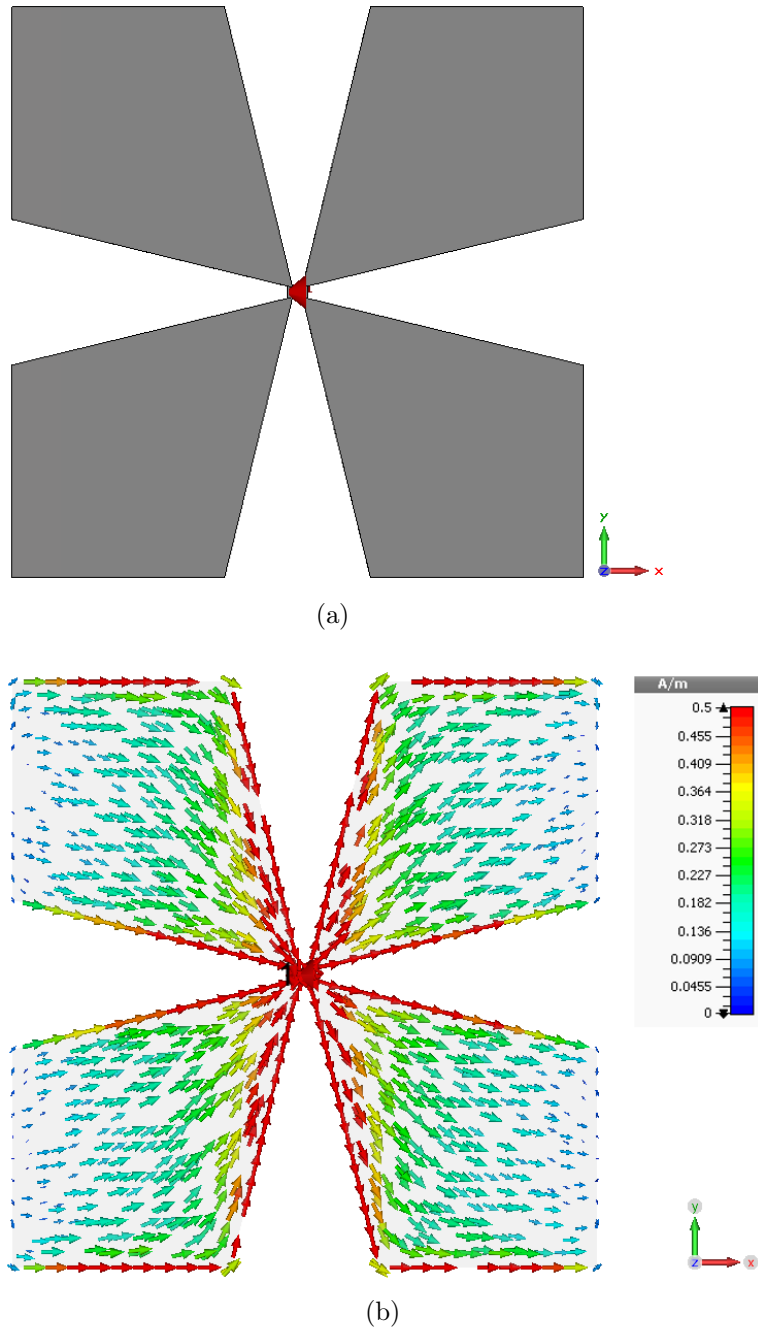


Figure 4.9: (a) Geometry of the 4sl petal board. (b) Current distribution of the 4sl at 600 MHz at a phase. Currents of the 4sl concentrate on edges again like the 4sq and the 4sl.

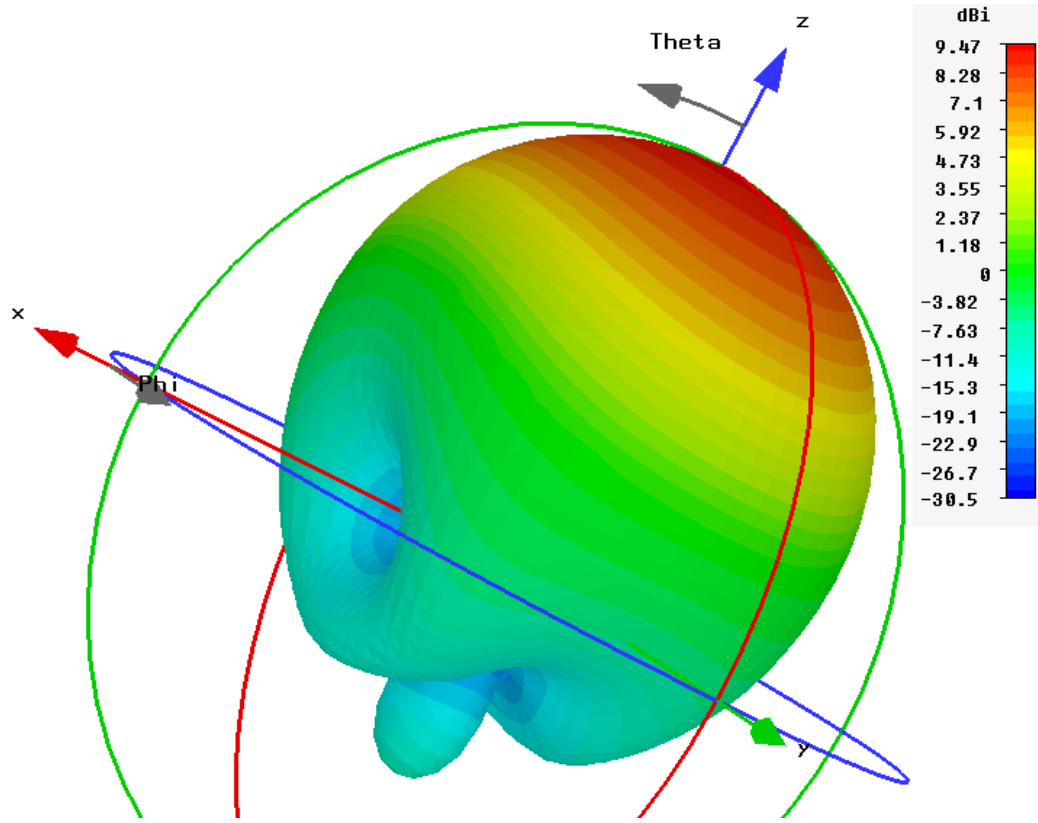


Figure 4.10: 3D representation of 4sl's beam at 600 MHz. E plane's beam width is 53.7° . H plane's beam width is 73.7° .

4.1.3 Comparison of Different Feeds

Table 4.1 shows the Half Power Beam Width (HPBW) comparison on both E plane and H plane among the 4sq, the 4pt and the 4sl at 600 MHz. It can be seen that beam patterns of these feeds are very similar to each other. This small difference does not make a preference to one feed than another. This similarity is also reasonable since wavelength is 500mm at 600 MHz, which is 2 or 3 times the size of petal board. So modifications of petal board is small compare to wavelength and cannot be seen strongly in beam pattern.

The conclusion is that: modifications of 4sq's petal board usually do not hurt the smooth and broad beam pattern and might be applied to have wider bandwidth without penalty.

4.2. Input Impedance of Single 4sq

Table 4.1: HPBW comparison among the 4sq, 4pt and 4sl.

| models | 4sq | 4pt | 4sl |
|-----------------------|------|------|------|
| E plane width(degree) | 58.3 | 55.9 | 53.7 |
| H plane width(degree) | 85.8 | 77.7 | 73.7 |

4.2 Input Impedance of Single 4sq

Input impedance is a key item that needs to be improved from existing feeds. Right now it is the stage to explore CST to reproduce the return loss of a known feed, the 4sq. So that CST's ability to simulate CHIME feed can be verified and used for designing.

4.2.1 Petal Board Model and Impedance Transformation

It is already known that the 4sq consists of a radiating petal board followed by balancing transmission lines all the way to SMA ports. In the ideal picture, only the petal board needs to be simulated, then impedance transformation theory can be applied to calculate the impedance at SMA ports from impedance at petal board. This saves lots of simulation time comparing with models which include all components of the 4sq. Therefore, petal board model is firstly tried together with impedance transformation to get impedance spectra.

Transmission Line Theory

A transmission line is a usually a long uniform structure, such as a cable, to carry radio wave. The length of transmission line is comparable to wavelength so circuit theory cannot be used directly. On the other hand, EM fields on a transmission line usually only vary in one dimension, so there is no need to solve field equations in 3D space. [17].

The scheme of a transmission line is shown in Fig. 4.11 (a). It extends uniformly in the x-axis direction to carry EM wave. An equivalent lumped element circuit of a small length Δx of transmission line is shown in Fig. 4.11 (b).

4.2. Input Impedance of Single 4sq

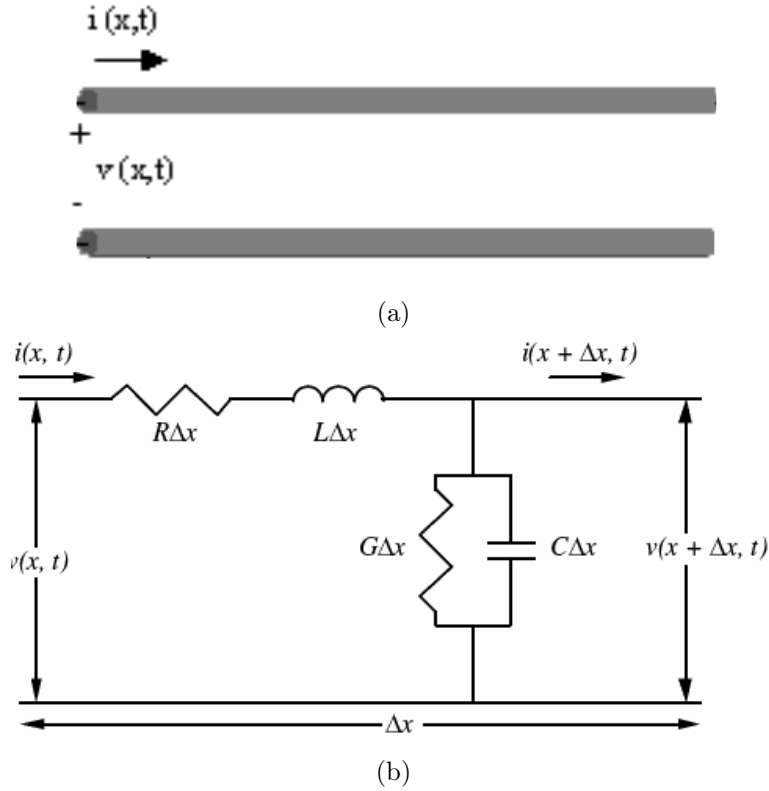


Figure 4.11: (a) Geometry of a part of a transmission line aligned in the x-axis. (b) Lumped element model for Δx long transmission line. Image source: http://en.wikibooks.org/wiki/Communication_Systems/Wired_Transmission.

Apply Kirchoff's law to the lumped circuit:

$$v(x, t) - R\Delta x i(x, t) - L\Delta x \frac{\partial i(x, t)}{\partial t} = v(x + \Delta x, t) \quad (4.1a)$$

$$i(x, t) - G\Delta x v(x + \Delta x, t) - C\Delta x \frac{\partial v(x + \Delta x, t)}{\partial t} = i(x + \Delta x, t). \quad (4.1b)$$

Divide Eq. 4.1 by Δx and take the limit that $\Delta x \rightarrow 0$ we get:

$$\frac{\partial v(x, t)}{\partial x} = -Ri(x, t) - L \frac{\partial i(x, t)}{\partial t} \quad (4.2a)$$

$$\frac{\partial i(x, t)}{\partial x} = -Gv(x, t) - C \frac{\partial v(x, t)}{\partial t}. \quad (4.2b)$$

4.2. Input Impedance of Single 4sq

This is called the telegrapher equation or transmission line equation in the time domain.

In the frequency domain, where EM wave is in sinusoidal steady-state condition, $i(x, t) = i(x)e^{j\omega t}$ and $v(x, t) = v(x)e^{j\omega t}$, Eq. 4.2 can be rewritten as

$$\frac{dv(x, t)}{dx} = -(R + j\omega L)i(x, t) \quad (4.3a)$$

$$\frac{di(x, t)}{dx} = -(G + j\omega C)v(x, t). \quad (4.3b)$$

From Eq. 4.3, voltage and current can be solved:

$$\frac{d^2v(x)}{dx^2} - \gamma^2v(x) = 0 \quad (4.4a)$$

$$\frac{d^2i(x)}{dx^2} - \gamma^2i(x) = 0, \quad (4.4b)$$

where $\gamma = \alpha + j\beta = \sqrt{(R + j\omega L)(G + j\omega C)}$. The solutions to Eq. 4.4 are

$$v(x) = V_0^+ e^{-\gamma x} + V_0^- e^{\gamma x} \quad (4.5a)$$

$$i(x) = I_0^+ e^{-\gamma x} + I_0^- e^{\gamma x}, \quad (4.5b)$$

$e^{-\gamma x}$ is the term of wave propagating forward while $e^{\gamma x}$ is the term of wave propagating backward. γ is the propagation factor of EM wave.

Combine Eq. 4.5 and Eq. 4.3:

$$Z_0 \equiv \frac{V_0^+}{I_0^+} = \frac{-V_0^-}{I_0^-} = \sqrt{\frac{R + j\omega L}{G + j\omega C}}. \quad (4.6)$$

The characteristic impedance Z_0 , determined by internal properties of the transmission line, equals the ratio of voltage's magnitude to current's magnitude when EM wave propagates only in one direction.

For a lossless transmission line, $R = G = 0$, then $Z_0 = \sqrt{LC}$ is purely real and independent of frequency. Meanwhile $\gamma = j\omega\sqrt{LC}$ is purely imaginary so that wave propagating along the transmission line does not attenuate in magnitude but only varies in phases.

To summarize, voltage and current propagation in a transmission line are

$$v(x) = V_0^+ e^{-\gamma x} + V_0^- e^{\gamma x} \quad (4.7a)$$

$$i(x) = \frac{V_0^+}{Z_0} e^{-\gamma x} - \frac{V_0^-}{Z_0} e^{\gamma x}. \quad (4.7b)$$

4.2. Input Impedance of Single 4sq

Z_0 represents the properties of transmission line itself. There are forward wave $e^{-\gamma x}$ and backward wave $e^{\gamma x}$ whose magnitude are respectively V_0^+ and V_0^- .

The relative magnitudes of V_0^+ and V_0^- are determined by the boundary condition of a transmission line, ie, the end configuration. For example, Fig. 4.12 shows a transmission line ended with a load Z_L .

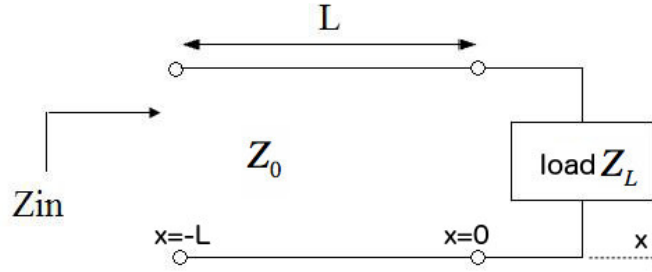


Figure 4.12: Load impedance Z_L is transformed to Z_{in} by a transmission line with length L and characteristic impedance Z_0 . Image source: <http://www.antenna-theory.com/basics/impedance.php>

At $x = 0$, apply circuit theory and Eq. 4.7, we get

$$Z_L = \frac{v_{x=0}}{i_{x=0}} = \frac{V_0^+ + V_0^-}{V_0^+ - V_0^-} Z_0. \quad (4.8)$$

This gives

$$\Gamma \equiv \frac{V_0^-}{V_0^+} = \frac{Z_L - Z_0}{Z_L + Z_0}, \quad (4.9)$$

where Γ is the reflection coefficient, defined as the ratio of backward wave to forward wave.

If length of the transmission line is l , the input impedance Z_{in} is

$$Z_{in} \equiv \frac{v_{x=-l}}{i_{x=-l}} = \frac{e^{j\gamma l} + \Gamma e^{-j\gamma l}}{e^{j\gamma l} - \Gamma e^{-j\gamma l}} Z_0 = Z_0 \frac{Z_L + jZ_0 \tan(\gamma l)}{Z_0 + jZ_L \tan(\gamma l)}. \quad (4.10)$$

Eq. 4.10 is the very important impedance transformation equation to transform the load impedance to the input impedance of a transmission line. If multiple transmission lines are along the way from load to input, Eq. 4.10 should be applied in sequence.

Application of Impedance Transformation to CHIME 4sq

Based on the impedance transformation theory discussed above, the procedure to apply it for 4sq's input impedance is:

1. simulate impedance of a pair of petals at the intersection between the petal board and stem boards by setting up a CST petal board model;
2. calculate shunt impedance at intersection between the petal board and stem boards when look into the transmission line formed by bottom layers of adjacent stem boards;
3. calculate the characteristic impedance of microstrip transmission lines;
4. parallelize petal impedance and shunt impedance to get load impedance of microstrip transmission lines;
5. apply Eq. 4.10 step by step, depending on how many stages of microstrips are along baluns, to get Z_{in} at SMA port; and
6. parallelize Z_{in} with itself from previous step.

For step 1, the model is the same as Fig. 4.1, except that this is the impedance of a pair of four petals. It needs to be doubled to get impedance of a pair of two petals; for step 2, the transmission line is short-loaded at baseboard and a rough estimate of shunt impedance can be made by an analytical calculation of a parallel plate transmission line; for step 3, characteristic impedance of a finite width microstrip is calculated by using empirical equations provided by Rogers ⁹; for step 6, Z_{in} is parallelized with itself because there is another parallel path from petal board to SMA from in-pair feeding. After step 6, transformed impedance at SMA is compared to measurement, as shown in Fig. 4.13. There is clearly disagreement.

⁹<https://www.rogerscorp.com/documents/783/acm/Design-Data-for-Microstrip-Transmission-Lines-of-TMM-Laminates.pdf>

4.2. Input Impedance of Single 4sq

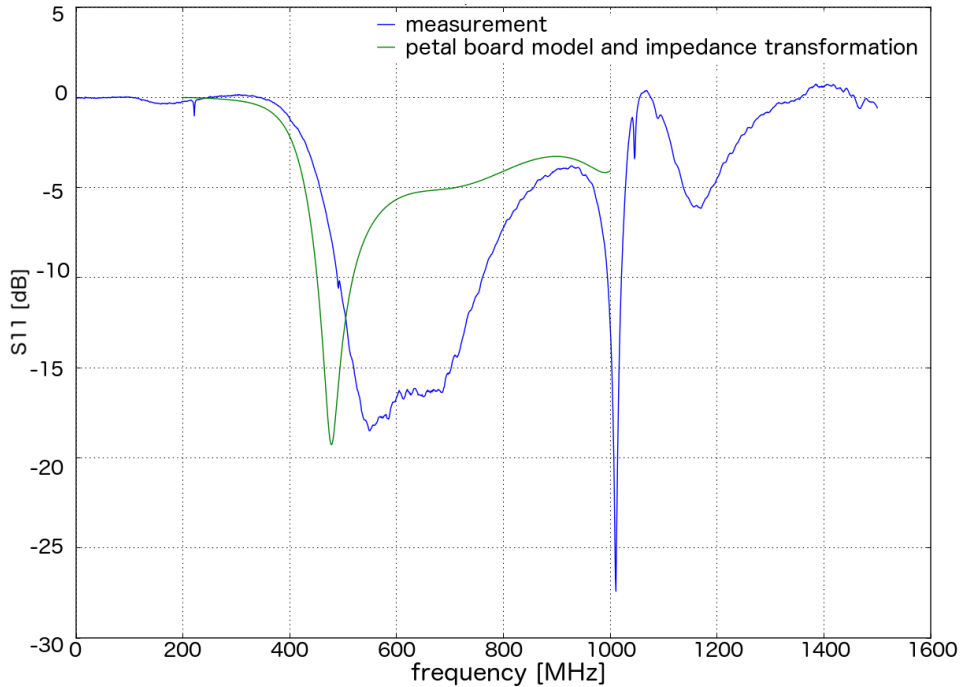


Figure 4.13: Comparison of 4sq's return loss between measurement and impedance transformation method (transformed from simulated impedance at the petal board).

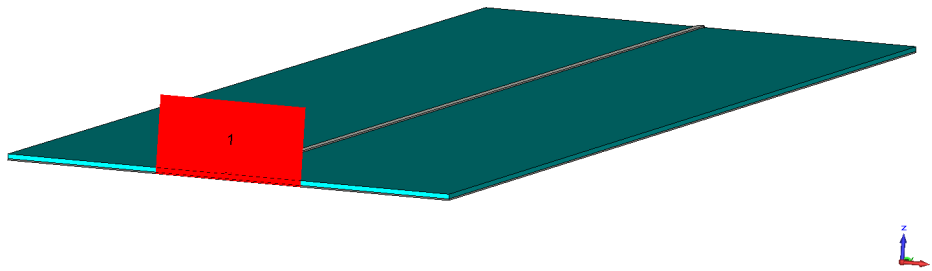
Coupling and Conclusions

Efforts have been made step by step to figure out reasons for the disagreement on 4sq's return loss between measurement and the impedance transformation method.

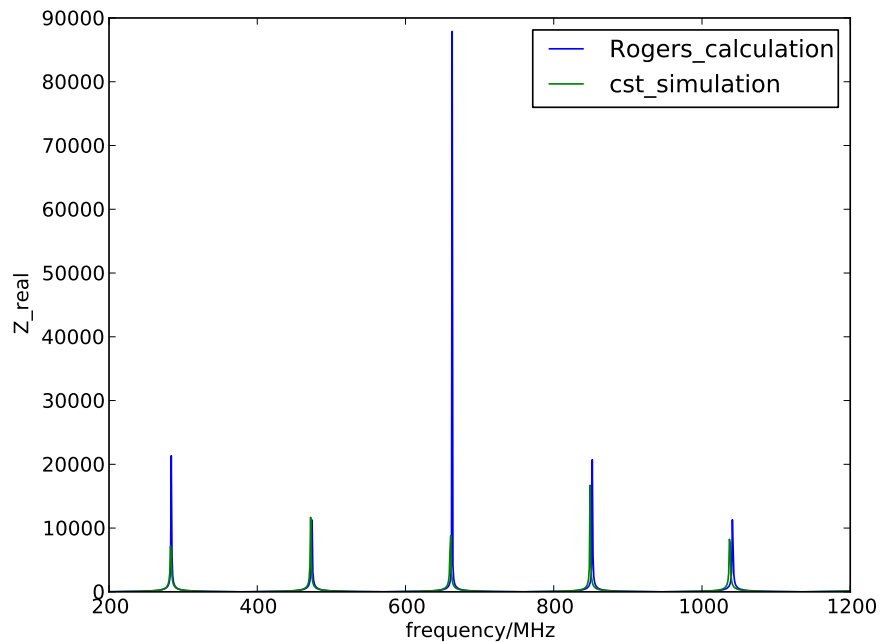
First, it is found that this disagreement is not due to inaccurate estimation of shunt impedance, because no matter how I change shunt impedance and even I exclude it, return loss given by impedance transformation method is almost the same.

Second, validity of Rogers' empirical equations and CST impedance simulation has been checked by simulation of a single short-loaded microstrip, as shown in Fig. 4.14 (a). Simulated input impedance is compared with impedance calculated from Rogers equation, as shown in Fig. 4.14 (b). Their match confirms both CST simulation and Rogers' empirical formula.

4.2. Input Impedance of Single 4sq



(a)



(b)

Figure 4.14: Input impedance of a single short-ended microstrip transmission line, given by both simulation and Rogers' analytical solution. (a) A model to simulate the input impedance of a short-ended microstrip transmission line. (b) Real part of input impedance comparison between simulation and empirical equation given by Rogers.

4.2. Input Impedance of Single 4sq

With the previous two points in mind, validity of impedance transformation method itself in the context of the 4sq needs to be checked. Therefore, the simplest impedance transformation configuration, which is a petal board fed by one microstrip in the center and a waveguide port feeding the other end of microstrip to get Z_{in} there, has been set up, as shown in Fig. 4.15. Input impedances of this configuration are simulated with length of microstrip to be 100 mm, 400 mm and 600 mm respectively. Except for direct simulation, there are another three ways to get Z_{in} of the 600 mm configuration.

First, use a 600 mm long microstrip to transform input impedance from petal board. Second, use a 500 mm long microstrip to transform input impedance from the 100 mm configuration. Third, use a 200 mm long microstrip to transform input impedance from the 400 mm configuration. All these three transformed Z_{in} are compared with the directly simulated result, as shown in Fig. 4.16.

The disagreement shown in Fig. 4.16 (a) and the agreement in Fig. 4.16 (c) proves that there is strong coupling between the petal board and microstrip, making the part of microstrip close to petal board not an ideal transmission line. Comparison between Fig. 4.16 (b) and Fig. 4.16 (c) shows that the further the microstrip's part, the less the coupling. Recall that the analysis of voltage and current distribution on transmission line is based on the assumption that transmission line is pretty long and isolated and its EM behaviour is not affected by anything else, it is understandable that the coupling between petal board and microstrip degrades the validity of applying impedance transformation for the 4sq. Further analysis proves that there is also strong coupling between stem boards and the baseboard.

4.2. Input Impedance of Single 4sq

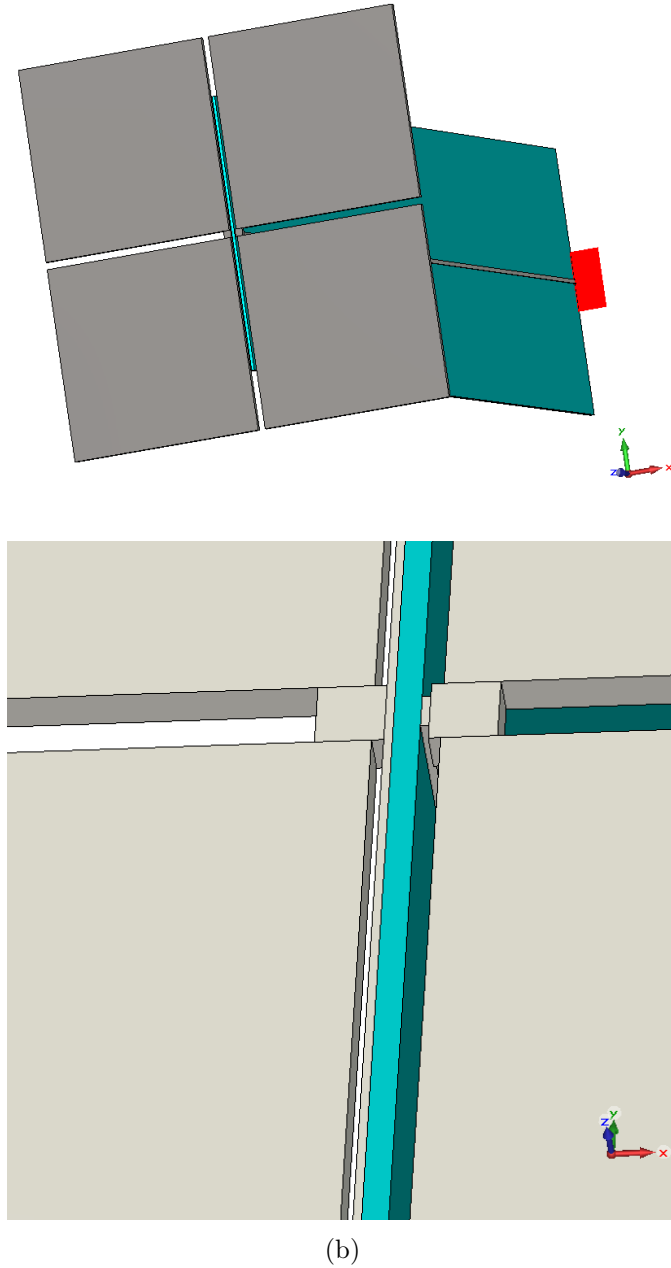


Figure 4.15: (a) Perspective view of a one-stage microstrip feeding the 4sq petal board. (b) Details on how microstrip feeds the petal board.

4.2. Input Impedance of Single 4sq

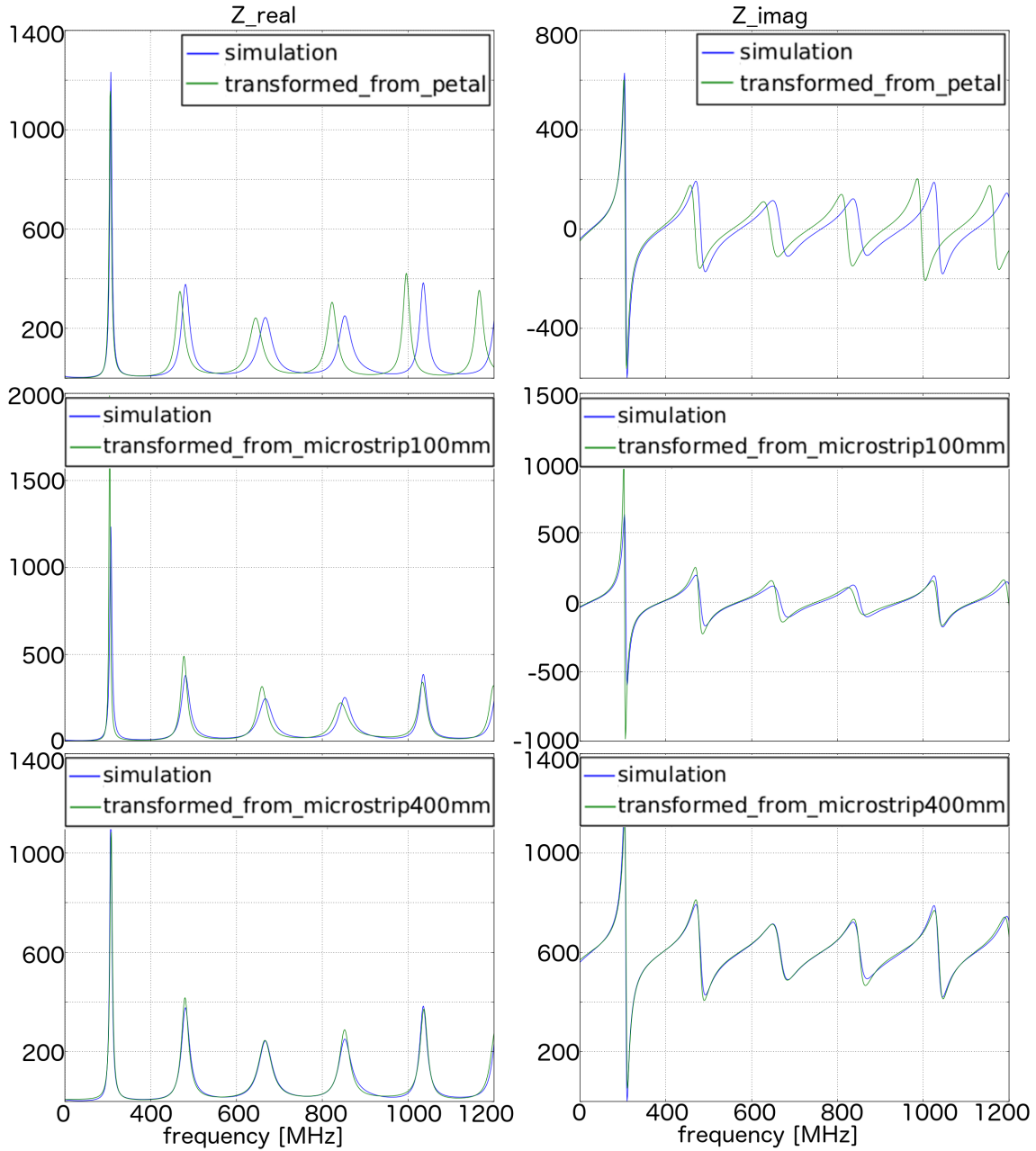


Figure 4.16: (a) Simulated Z_{in} of the 600 mm configuration are compared with (a) impedance transformed from petal board, (b) impedance transformed from the 100 mm configuration, (c) impedance transformed from the 400 mm configuration. Left panel is Z_{real} and right panel is Z_{imag} . The conclusion is: there is strong coupling between the petal board and microstrip.

The existence of shunt impedance and in-pair feeding makes any trial to simulate part of the 4sq and to include couplings at the same time not possible.

4.2.2 Full Feed Model

The impedance spectra given by the petal board model simulation and an impedance transformation are wrong because they ignore multiple couplings around. Thereafter, a full 4sq model has been constructed, as shown in Fig. 4.17 (a). A full detailed 4sq model cannot be managed by CST, since it costs lots of memory to represent the details. Therefore, there are two important simplifications in the full feed model.

First, the traces on the baseboard are simplified to be clear and symmetric, as shown in Fig. 4.17 (b). Second, traces of only one polarization in present. This can be seen in both the baseboard construction and petal board construction, shown in Fig. 4.17 (c).

The first simplification is verified by my previous experiences with CST that traces' length on the base board has little effect on return loss, let alone how traces are distributed. The second simplification is verified by the return loss measurement that, no matter the other polarization is short, open or loaded, the return loss of the polarization under test is almost the same. Fig. 4.18 shows the return loss comparison between the full feed model simulation and VNA measurement. We can see that they agree pretty well with each other.

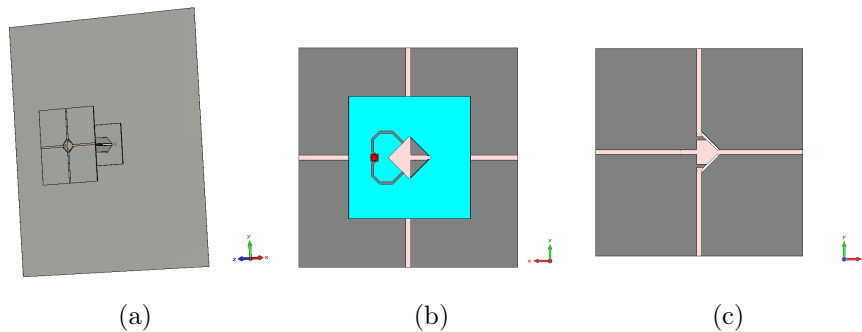


Figure 4.17: (a) Perspective view of the full 4sq model. (b) Simplified base board of the full 4sq model. (c) Petal board shows that only one polarization is present.

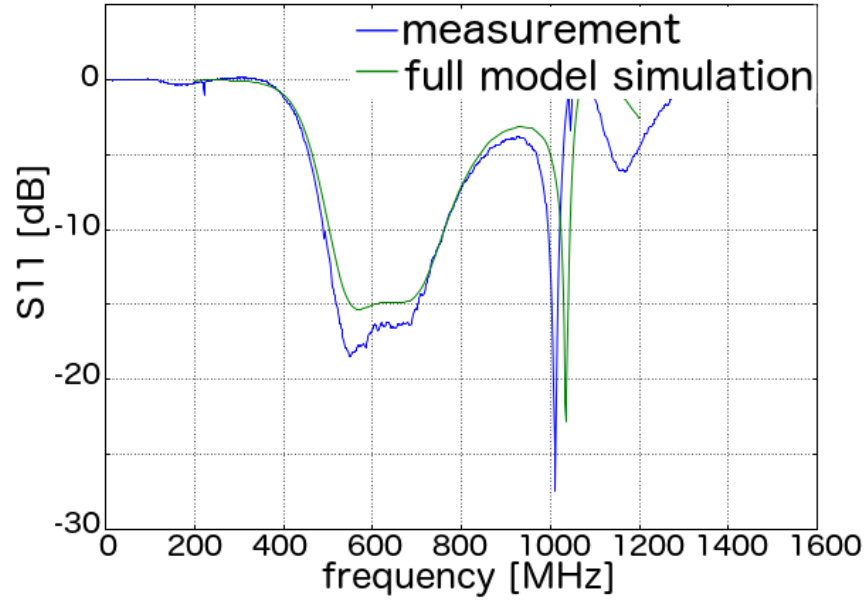


Figure 4.18: 4sq’s return loss comparison between the full 4sq model simulation and measurement. The agreement between these two proves the validity of full feed model to predict impedance spectra of the 4sq.

The full feed model, which has already been proved to be efficient to predict impedance spectra of the 4sq, will be applied for future CHIME feed design.

Chapter 5

The Cloverleaf Feed

5.1 Inspiration and Confirmation of the Cloverleaf Idea

Various modifications of the 4sq have been tried to make it wide-band, such as the 4pt, the 4sl. But they are all not satisfying due to narrow bandwidth or manufacture difficulty. A turning point in our approach occurred during a design discussion several of us had at the DRAO in which we realized that the Vivaldi antennas [18, 19], which are arrays of curved elements, have a much broader bandwidth than simple straight dipoles do. Recall that the current pattern of the 4sq is just like two straight dipoles facing each other, we realize that a Vivaldi-like 4sq might be broad band. To make the 4sq Vivaldi-like, it is straightforward to make its outer edges to be curved. From now on, a Vivaldi-like 4sq is called the cloverleaf antenna.

A cloverleaf feed in MOST band

To test the idea of cloverleaf feed, Duncan Campbell-Wilson added copper strips by hand to MOST 4sq to make its outer edges curved, as shown in Fig. 5.1 (a), its return loss measurement is shown in Fig. 5.1 (b) when an extra tuning short is added to the stem boards to improve impedance match. Without the extra tuning short on stem boards, the return loss is not that small but its shape across band is still broad. This experiment is very encouraging, confirming the cloverleaf feed is broad band, especially recall that this is a first-try handmade feed without any numerical design. Our belief is that a careful numerical design of petal shapes and/or baluns would make the cloverleaf feed wide band without tuning short.

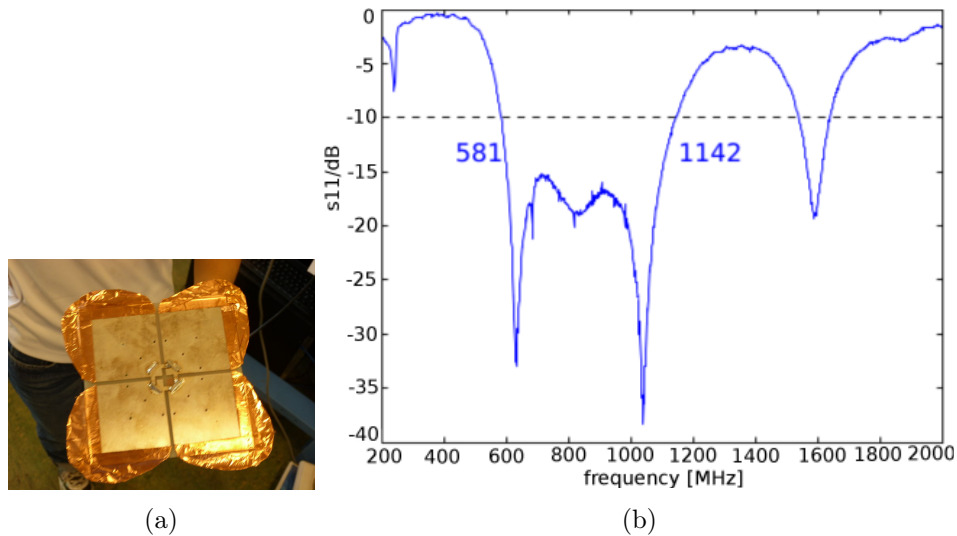


Figure 5.1: (a) A cloverleaf prototype hand built from MOST 4sq. Front view. (b) Measurement of the return loss of MOST cloverleaf feed after a tuning short is added to the stem boards. This experiment supports the idea that a cloverleaf antenna might be very broadband.

5.2 CHIME Cloverleaf Feed

5.2.1 Further Test of the Full Feed Model

To test the validity of full feed model for reproducing return loss of the cloverleaf feed, several cloverleaf feeds in CHIME band are built, measured and simulated.

First, we built a cloverleaf prototype by cutting metal sheet to be curved and balance it with CHIME 4sq baluns, as shown in Fig. 5.2 (a). A full feed model of this feed has been constructed in CST and simulation is compared to measurement as shown in Fig. 5.2 (b). The very good agreement between simulation and measurement reassures full feed model's validity in the CHIME feed design.

Then, a printed version of the cloverleaf feed is built but its return loss's measurement disagrees with the simulation. Later it is found that, the FR4 in the gap between petals has non-negligible effect on impedance at the petal board ports, causing disagreement to simulation which includes no dielectrics in petal board. Recall that current concentrates along 2 pairs of inner petal

edges, there is strong E field to see RF4 in the gaps and be affected by its dielectric constant. The difference between the cut-out prototype and printed prototype is just like the difference between transmission line filled with air and transmission line filled with FR4. After the FR4 gaps are removed, return loss measurement does agree with simulation.

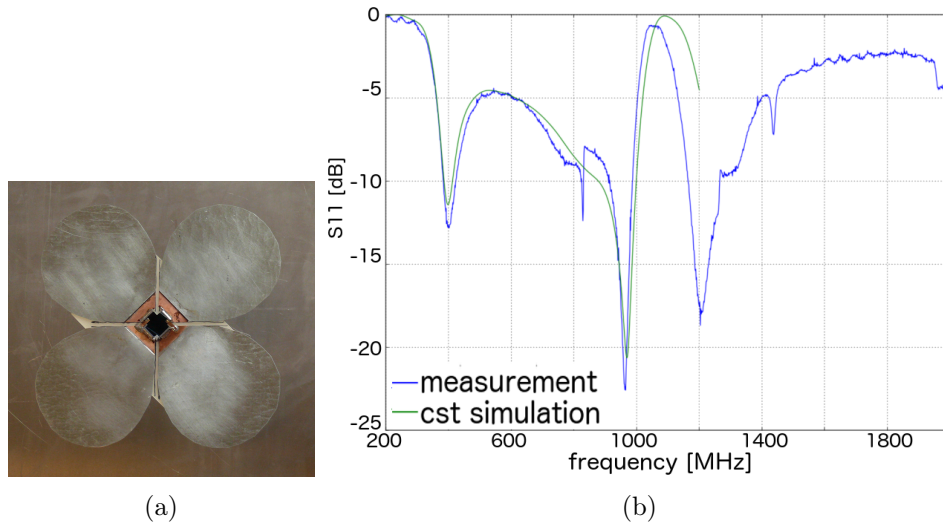


Figure 5.2: (a) A cloverleaf prototype in CHIME band. Front view. (b) Return loss comparison between measurement and simulation of the CHIME cloverleaf prototype. It confirms the full feed model simulation technique is applicable to the cloverleaf feed.

5.2.2 Cloverleaf Feed Design and Optimization

After further confirmation of full feed model technique, it is now the stage to apply this simulation technique for designing CHIME cloverleaf feed numerically.

The procedure is as follows:

1. use W, R, L to parametrize petal board, as shown in Fig. 5.3;
2. while fix baluns to be the 4sq baluns, optimize W, R, L until the smallest return loss across band is found; and
3. redesign the 2-stage 4sq baluns to have 3-stage transmission lines, at the optimal W, R, L found above, as shown in Fig. 5.4.

5.2. CHIME Cloverleaf Feed

In step 2, 4sq baluns are used only for manufacture convenience. Once some optimization result comes from step 2, a corresponding cloverleaf feed can be made easily to reassure everything is working as what we think, and it is. Another crucial designing note is that after optimization of petal shape, a new stage transmission line should be introduced in step 3 rather than continue optimizing the two-stage baluns for lower return loss, because the essence of step 2 is an optimization of petal shape to the two-stage transmission line which already exists. Any deviation of transmission line's parameters would make return loss worse except for introducing new freedom. This is exactly to make further use of the great flexibility of microstrip transmission lines compared to other types of transmission lines. Meanwhile the total length of transmission lines on stem boards should be kept the same to ensure a quarter wavelength separation between petal board and ground plane at central frequency 600 MHz.

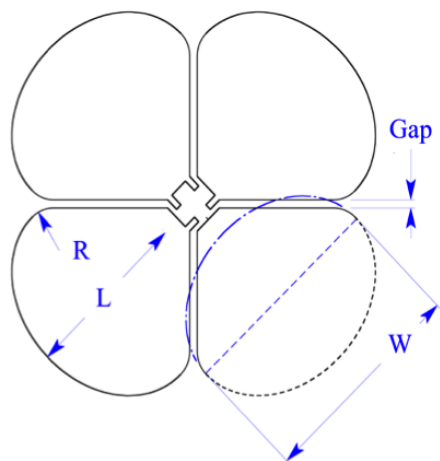


Figure 5.3: The shape of each petal consists of two perpendicular straight lines, two 45 degree circular arcs with radius R and one half an ellipse. W is the major axis of the ellipse and L is the length from the intersection of the straight sides to the outer edge of the ellipse. The shape is illustrated here for the adopted values of gap, R , L and W .

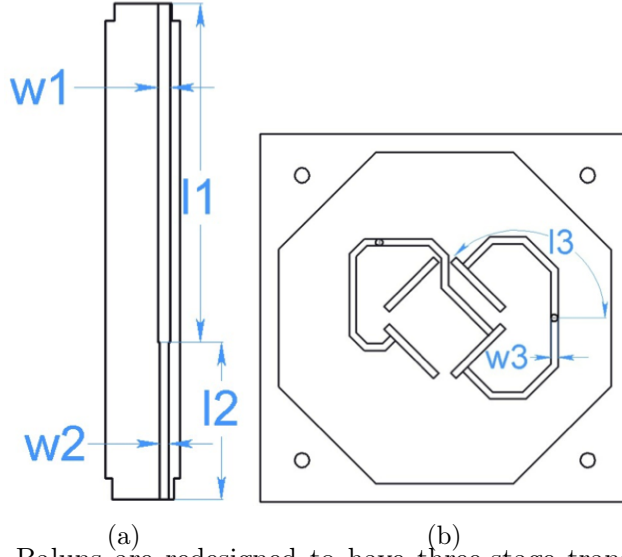


Figure 5.4: Baluns are redesigned to have three-stage transmission lines. Two of them are on stem boards, while the third is on baseboard. (a) A two-stage transmission line on stem boards, which are parametrized by $W1, L1$ and $W2, L2$. (b) A one-stage transmission line on base board, which is parametrized by $W3, L3$.

Finally, the designed parameters are in table 5.1.

Table 5.1: Designed parameters of the cloverleaf feed in CHIME band.

| parameters | W | L | R | W1 | L1 | W2 | L2 | W3 | L3 |
|--------------------|-------|-------|------|-----|------|-----|------|-----|------|
| designed value(mm) | 138.5 | 131.9 | 20.0 | 3.5 | 94.0 | 2.5 | 40.0 | 1.9 | 45.0 |

5.2.3 Realization of the Optimized Cloverleaf Feed Design

An cloverleaf feed is built according to the designed parameters, as shown in Fig. 5.5 (a). Fig. 5.5 (b) shows that the ports at center of the cloverleaf feed's petal board have been modified to have simpler and clearer geometry. The cloverleaf feed's return loss is measured and compared to simulation, shown in Fig. 5.6. There is a pretty good agreement between simulation and measurement. Return loss is smaller than -10dB return loss across the CHIME band, with majority of the band to be smaller than -15dB. Return

losses of the two polarizations are similar to each other because of careful design of traces on the baseboard to reduce coupling and to improve symmetry.

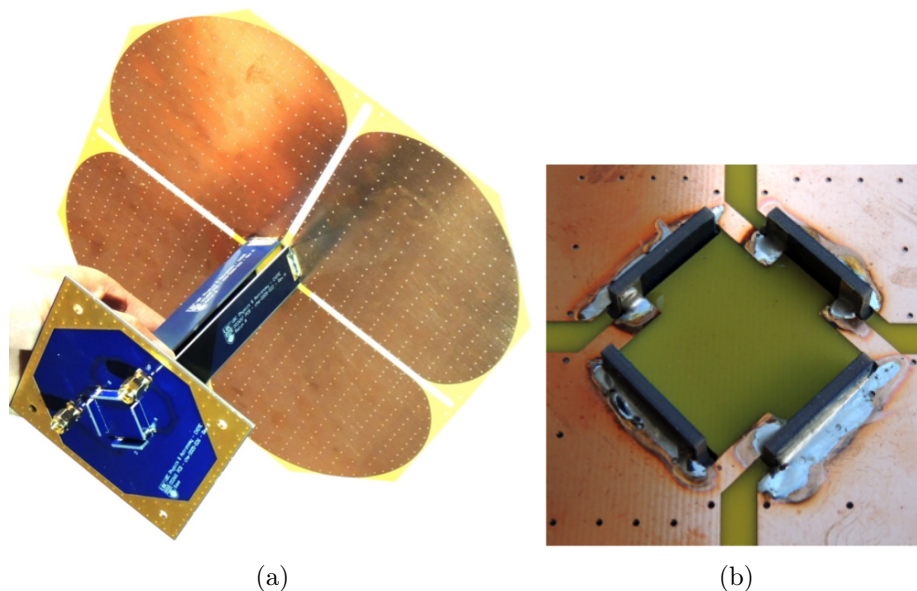


Figure 5.5: (a) Perspective view of the cloverleaf feed built with designed parameters. Note, the FR4 in gaps between the petals are removed but the far end is kept because it improves mechanical strength of the petal board quite a lot. (b) Modified port at the center of cloverleaf petal board to make the connections simpler.

Fig. 5.7 shows measurements of both E plane and H plane of this cloverleaf feed, which are done by Jeff Peterson at Carnegie Mellon University. The beam pattern is broad and smooth across the band, with only few side lobes in the backward direction. It is a confirmation of our understanding of beams in chapter 4 and also a confirmation of this design.

Furthermore, the largest dimension on petal board, which is the diagonal length, is 27 cm. Size of the cloverleaf feed is small enough to be placed at any azimuth angle in CHIME array. This cloverleaf feed consists of PCB boards, the same as the 4sq, so it should be strong enough to survive field environment. The existence of ground plane provides a mirror image of the feed so that phase centers of beams across the band all locate on the ground plane. The Teflon balun boards, the viaed double-layer petal board and

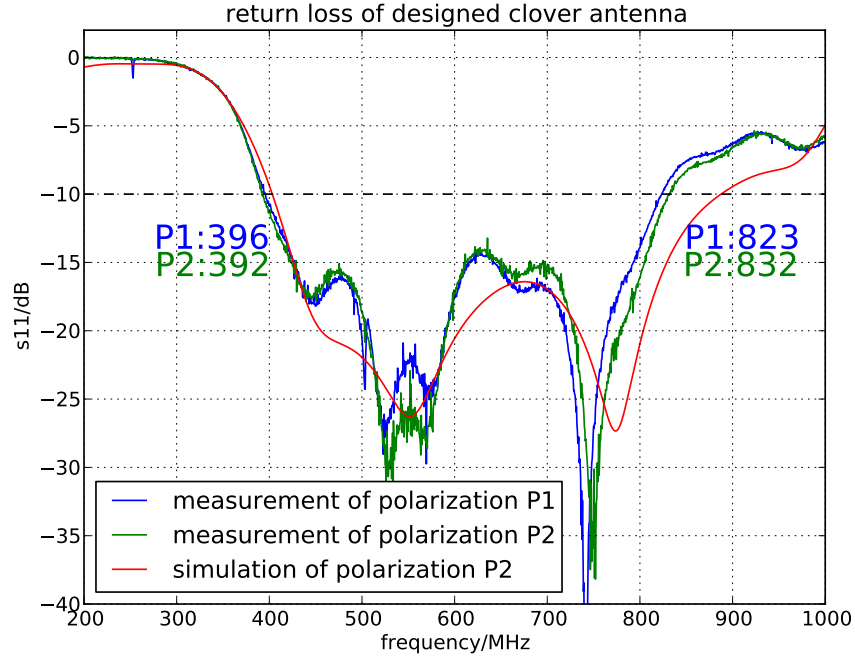


Figure 5.6: Return loss comparison between measurement and simulation of CHIME cloverleaf feed. The agreement between them confirms the validity of simulation and the very wide bandwidth shown in this figure confirms the design of the cloverleaf feed.

the removal of FR4 in the gap between petals together make the loss of the cloverleaf feed to be the smallest.

Up to now, all requirements of the CHIME feed, especially a very wide bandwidth, are satisfied by this cloverleaf design. So it is confirmed to be the final and will be mass produced and deployed on the CHIME pathfinder.

5.2. CHIME Cloverleaf Feed

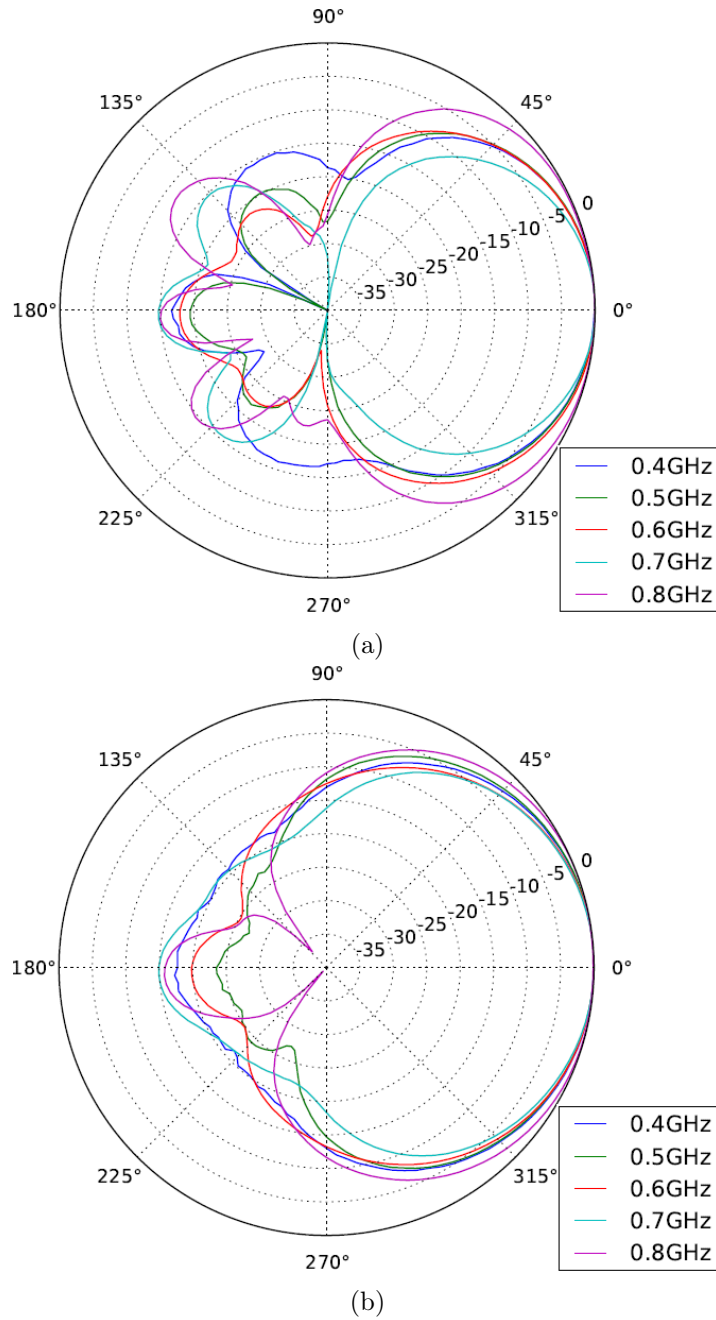


Figure 5.7: Measurement of co-polar beam pattern of the designed cloverleaf. They are smooth and broad across band, as required by CHIME. (a) E plane measurement of designed CHIME cloverleaf feed. (b) H plane measurement of designed CHIME cloverleaf feed

Chapter 6

Manufacture and Deployment of The Cloverleaf Feeds

The cloverleaf feed whose design has been expressed in the previous chapter has been built, measured and confirmed to be the CHIME feed. Therefore, it is mass produced and deployed on CHIME pathfinder to take sky data.

6.1 Specifications of the Designed Cloverleaf Feed

Followings are the specifications of designed cloverleaf.

- Parameters of microstrip traces and petal shape are displayed in Table 5.1.
- Additional structural specifications needed to manufacture the whole cloverleaf feed are shown in Fig. 6.1. All units are in mm.
- The FR4 in gaps between petals on the petal board are removed but the very out end are left, as can be seen in Fig. 5.5 (a) and Fig. 6.1 (c).
- 1 oz rolled copper is printed on both sides of FR4-supported petal board.
- Petal board is viaed.
- Baluns' dielectric material is chosen to be Arlon DiClad 880, which is low-loss, cheap, with dielectric constant around 2.2.
- The thickness of balun boards is 1.57 ± 0.13 mm.

The FR4 in very out end of gaps are left to make petal board stronger. Rolled copper rather than electro-deposited copper is chosen because the former is less lossy, more smooth on the surface and the prices of these two do not differ too much.

6.1. Specifications of the Designed Cloverleaf Feed

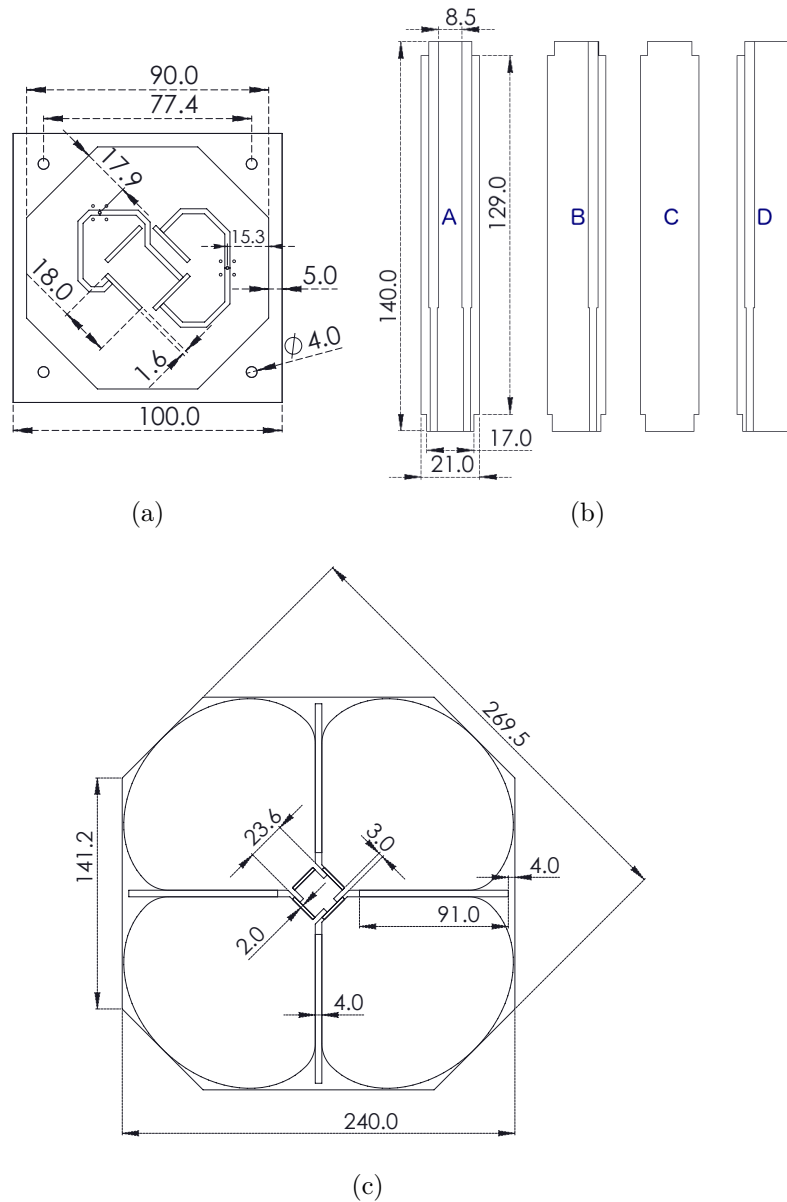


Figure 6.1: Manufacture dimensions of the designed cloverleaf feed. (a) Dimensions of baseboard. (b) Dimensions of 4 stem boards. Stem A has two traces, while stem C has none. This is set by the geometry for in-pair feeding. (c) Dimensions of petal board.

6.2 Manufacture Process

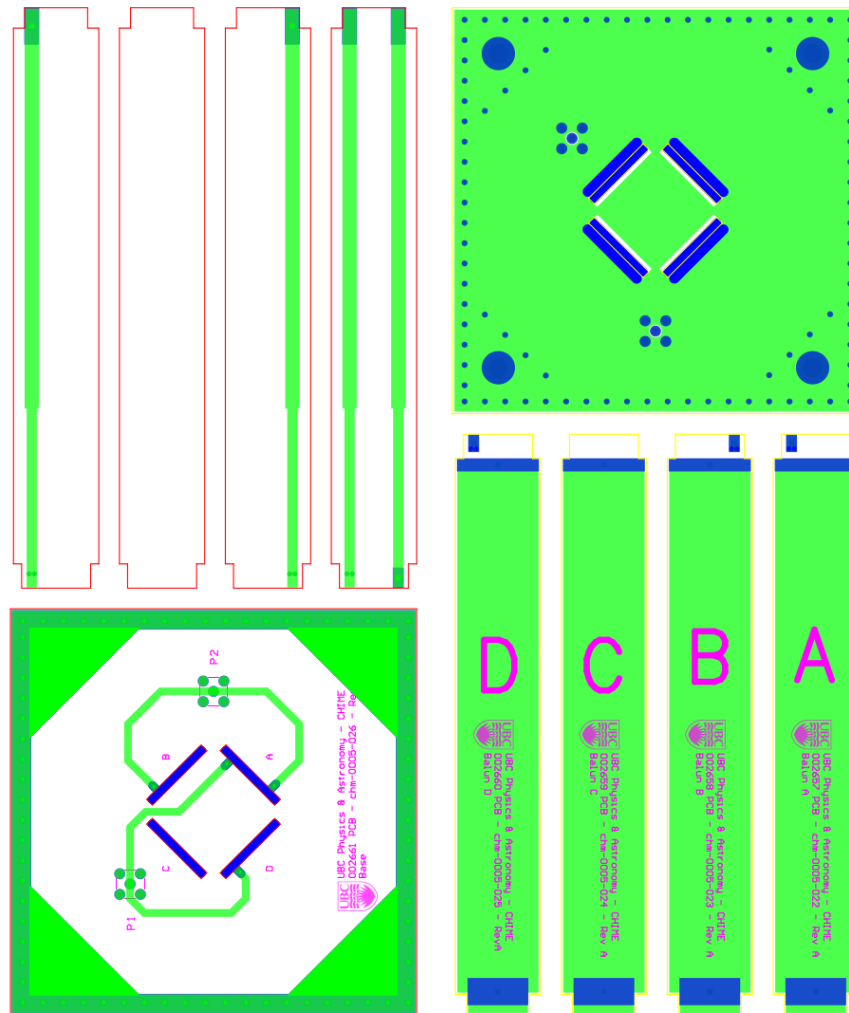
To get mass production of cloverleaf feeds, I exported geometries of the cloverleaf feed from CST in dxf files. With great help from Richard Lam, dxf files were transformed to Gerber files, which are the standard format for manufacture companies. 132 sets of petals were ordered from Canadian Circuits and 132 sets of baluns were ordered from Enigma. These two companies are different because different substrates are needed for balun boards and petal boards. Enigma helped to penalize stem boards and baseboards together to reduce material waste. The panel is shown in Fig. 6.2. The cost of boards for each feed is around 120 dollars. This number will be reduced to 80 dollars for full CHIME because 1280 feeds instead of 132 feeds will be ordered. We assembled 128 feeds from PCB boards by using a jig, as shown in Fig. 6.3. It takes around 2 minutes to assemble a feed from PCB boards. Each feed was tested in the lab with the VNA to see whether it is working properly. Table 6.1 illustrates how we tested each feed. All the cloverleaf feeds passed the test successfully and were deployed as feed array on the focal lines of CHIME pathfinder, as shown in Fig. 6.4.

Table 6.1: Details on The Cloverleaf Feeds' Acceptance Test.

| | |
|-----------------------------|---|
| test setup | VNA is calibrated and the same configuration is applied for every feed under test |
| test procedure | mount a feed to a 1.5 m high pole, where feed's orientation can be changed ; connect the 2 outputs of 2 polarizations to the 2 ports of VNA; measure S11 and S22 in the frequency range [400MHz, 800MHz]; make a judgment on whether the feed pass the test by visualization. |
| pass criteria ¹⁰ | S11 and S22 were less than -2dB, in the range [400MHz, 450MHz]; S11 and S22 were less than -5dB, in the range [450MHz, 500MHz]; S11 and S22 wre less than -10dB, in the range [450MHz, 650MHz]; S11 and S22 were smaller than -15dB around 600MHz; S11 and S22 exhibited interaction with the room environment as demonstrated by significant changes with feed's orientation |

¹⁰feed passes the test if an orientation can be found in which S11 and S22 satisfy all the criteria listed in the right side.

6.2. Manufacture Process



(a) Top view of panelized boards (b) Bottom view of panelized boards

Figure 6.2: Panelization of base boards and stem boards to reduce material waste.

6.2. *Manufacture Process*

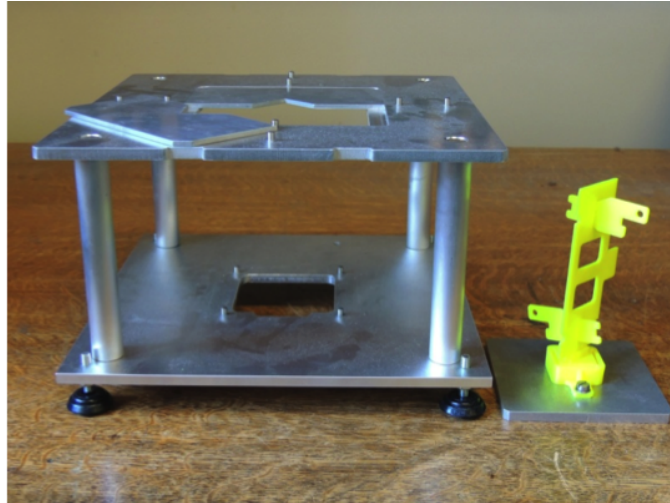


Figure 6.3: A jig for assembling the cloverleaf feeds.



Figure 6.4: The cloverleaf feeds installed on CHIME pathfinder as feed array.

6.3 Sky Data Taken from Deployed Cloverleaf Feeds

To have an preliminary test the cloverleaf feed's performance on the reflector, the pulse from the pulsar PSR B0329+54 was measured, as shown in Fig. 6.5. The cloverleaf feeds on the reflector sees that the arriving time of the signal varies with frequency due to dispersion of galactic matter. It is a proof that the cloverleaf feeds are working properly across the band.

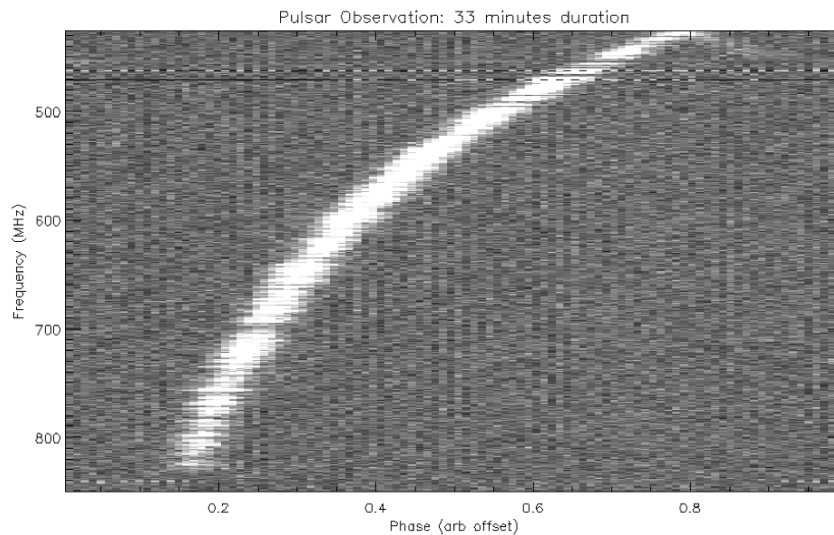


Figure 6.5: One pulse measurement of the pulsar B0329+54 from the cloverleaf feed on the CHIME pathfinder. The phase range of X-axis corresponds to the period of the pulsar, which is 0.7 s. The measured arriving time of signal depends on frequency. This is a sign of galactic matter's dispersion and a sign of good performance of the cloverleaf feed cross band.

To measure the shape of reflector beams, holography has been applied between CHIME pathfinder and the 26m Telescope at DRAO for a Cas A¹¹ transit. The 26m telescope was tracking Cas A during the period when data were taken. Observed data displayed in Fig. 6.6 agrees with several common senses, which are: signal should have fringes in the time domain because there is East-West baseline between CHIME pathfinder and the 26m Telescope; the fringe should be finer for a higher frequency and width

¹¹http://en.wikipedia.org/wiki/Cassiopeia_A.

6.3. Sky Data Taken from Deployed Cloverleaf Feeds

of reflector beams should be finer for a higher frequency. Moreover, shape of reflector beams, as indicated by red dots, exhibit a generally normal shape, which can be fitted by a Gaussian distribution in the main lobe. Therefore, the cloverleaf feeds are working well.

To have an idea of what the reflector beam would look like on the full sky, a Grasp model has been constructed in which pathfinder's reflector is fed by the beam pattern of a cloverleaf feed. The simulated co-polar beam on the full sky is shown in Fig. 6.7 (a). Since cylindrical reflector is aligned north-south, it is reasonable to see the beam elongated in north-south direction. Reflector beams' widths in the slice of CasA transit are compared between measurement and simulation, as shown in Fig. 6.7 (b). The agreement there is a confirmation of my simulation and also a confirmation of our preliminary understanding of our beams.

6.3. Sky Data Taken from Deployed Cloverleaf Feeds

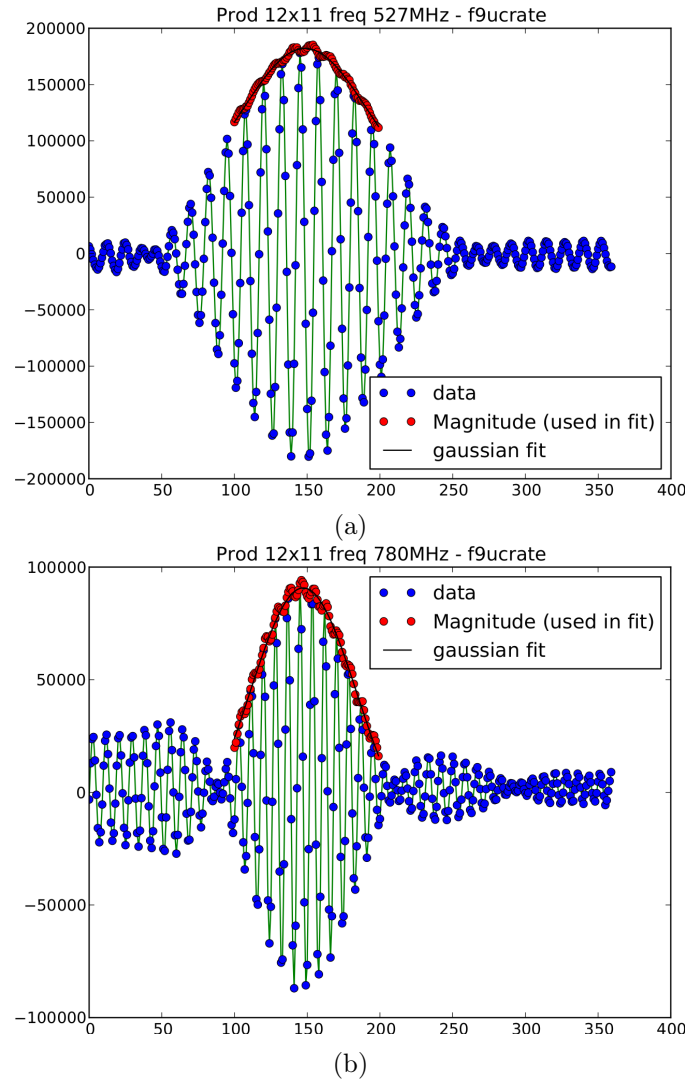


Figure 6.6: Cross correlations between DRAO's 26m Telescope and CHIME pathfinder when Cas A transited through CHIME pathfinder's field of view. Both reflectors are fed with the cloverleaf feeds. x-axis is linearly mapped to time. Its spans 3600 s. (a) cross correlation at 527 MHz. (b) cross correlation at 780 MHz. The fringes are clear as shown by the data points. Shape of reflector beams are generally good, as indicated by red dots. Comparison between (a) and (b) shows that the width of reflector beams and spacing of fringes depend on frequency. Image Credit: Mateus Fandino.

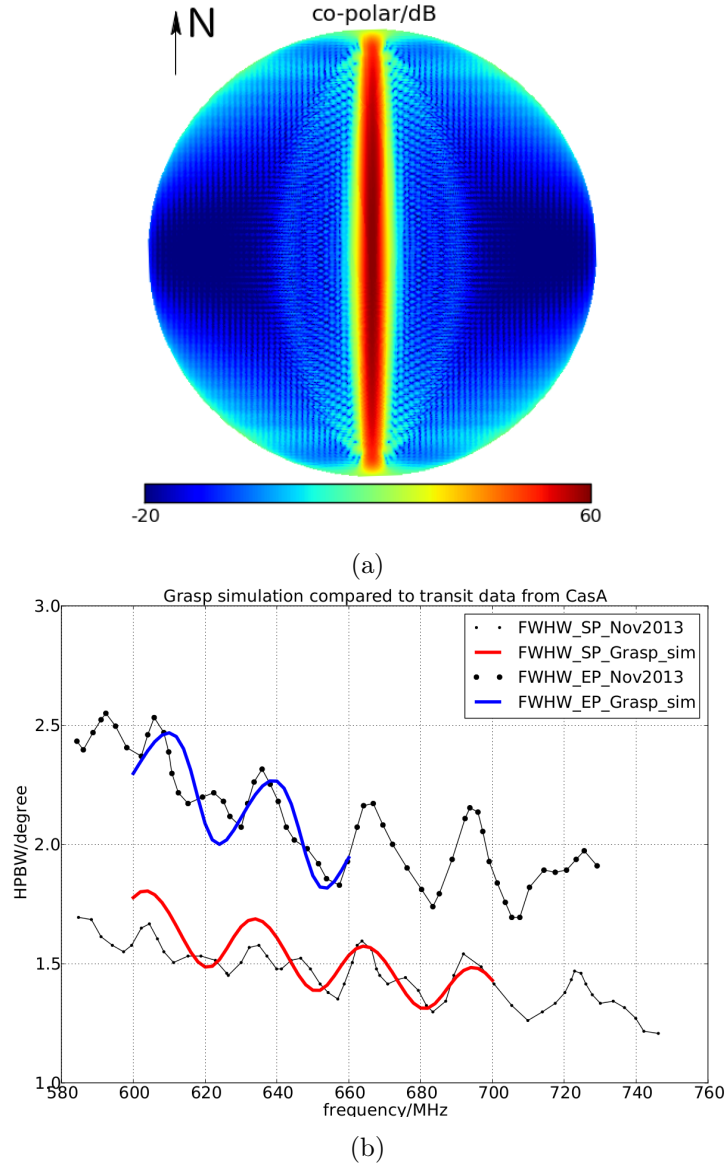


Figure 6.7: (a) Grasp simulated co-polar reflector beam at 600 MHz. (b) Simulated beam widths in the slice of CasA transit are compared to measurements for north-south polarization and east-west polarization of the cloverleaf feed.

Chapter 7

Conclusion

The cloverleaf antenna designed in this thesis meets all the feed requirements of CHIME, especially the very wide bandwidth requirement.

Because of the very good performance of the cloverleaf antenna, CHIME feed becomes finalized as a fixed element in the whole experiment. This removes large uncertainty of CHIME and smooths the whole procedure. CHIME's foreground removal strategy, which once was based on an over-simplified assumption of feed's beam pattern, can be evaluated realistically since CHIME's feeds and all properties related with them are now real data. Because impedance spectra of the cloverleaf feed as the CHIME feed are known and fixed, an effective approach to lower system temperature now becomes clear: redesign LNA to have minimal noise at the cloverleaf feed's impedance spectra. The performance of reflector can be studied directly in terms of beams to the sky because the feed, as an input to reflector beams, is well understood, good enough and finalized. For example, centroids of reflector beams are measured to wander east-west across band. The mechanism of wandering is not understood yet. But we have made sure wandering comes from reflector rather than feeds because 180 degree azimuthal rotation of feed does not result in a 180 degree phase change in the centroid spectrum.

Without cloverleaf feeds, feeds with bad performance have to be installed, making CHIME pathfinder to be less useful. For example, feeds with narrow bandwidth harm the system behavior across the band so that dispersion of galactic matter might not be seen from pulsar measurement. Feeds with large size exclude the configuration of feed array in which each element is azimuthally rotated 45 degree so that we lose the chance to analyze the behavior of pathfinder whose reflector beams between two polarizations are the same. Feeds which introduce high system temperature reduce SNR, making CHIME pathfinder's sky mapping more time consuming or even not possible.

In conclusion, the successful design of the cloverleaf feed is a real progress for CHIME.

Moreover, the idea and design procedure of cloverleaf feeds can be easily tuned to other bandwidth for other usage. Actually, designing a similar

cloverleaf feed for MOST is already on the task list.

The next step is to use Grasp to analyze the interaction between feed and reflector to get reflector beams on the sky. It has been confirmed already by both simulation and measurement that widths of reflector beams oscillate with frequency with 30 MHz ripples because there is an extra bounce of beams between reflector and focal line. Slices of beams have been measured by using pulsar and other bright radio sources. It needs intensive effort to integrate measured beam slices to simulated 3D beams based on their accuracy level.

Cross talk between element in the deployed feed array is another topic needs future analysis.

Bibliography

- [1] Kevin Bandura, Graeme E Addison, Mandana Amiri, J Richard Bond, Duncan Campbell-Wilson, Liam Connor, Jean-Francois Cliche, Greg Davis, Meiling Deng, Nolan Denman, et al. Canadian hydrogen intensity mapping experiment (chime) pathfinder. In *SPIE Astronomical Telescopes+ Instrumentation*, pages 914522–914522. International Society for Optics and Photonics, 2014.
- [2] Adam G. Riess et al. Observational evidence from supernovae for an accelerating universe and a cosmological constant. *Astron. J.*, 1998.
- [3] Saul Perlmutter, G Aldering, G Goldhaber, RA Knop, P Nugent, PG Castro, S Deustua, S Fabbro, A Goobar, DE Groom, et al. Measurements of Ω and Λ from 42 high-redshift supernovae. *The Astrophysical Journal*, 517(2):565, 1999.
- [4] P. J. E. Peebles and Bharat Ratra. The cosmological constant and dark energy. *Reivews of Modern Physics*, 2003.
- [5] Steen Hannestad and Edvard Mörtsell. Probing the dark side: Constraints on the dark energy equation of state from cmb, large scale structure, and type ia supernovae. *Phys. Rev. D*, 66:063508, Sep 2002.
- [6] Adam G Riess, Louis-Gregory Strolger, Stefano Casertano, Henry C Ferguson, Bahram Mobasher, Ben Gold, Peter J Challis, Alexei V Filippenko, Saurabh Jha, Weidong Li, et al. New hubble space telescope discoveries of type ia supernovae at $z \lesssim 1$: narrowing constraints on the early behavior of dark energy. *The Astrophysical Journal*, 659(1):98, 2007.
- [7] J. Richard Shaw. All-sky interferometry with spherical harmonic transit telescope. *The Astrophysical Journal*, 2014.
- [8] Gregory Davis. A two element interferometer prototype for the canadian hydrogen intensity mapping experiment. Master’s thesis, University of British Columbia, 2009.

Bibliography

- [9] J.R. Nealy C.G. Buxton, W.L. Stutzman. Analysis of a new wideband printed antenna element (the foursquare) using fdtd techniques. *URSI National Radio Science Meeting*, 1998.
- [10] Seong-Youp Suh, Warren Stutzman, William Davis, Alan Waltho, Kirk Skeba, and Jeffrey Schiffer. A novel low-profile, dual-polarization, multi-band base-station antenna element-the fourpoint antenna. In *Vehicular Technology Conference, 2004. VTC2004-Fall. 2004 IEEE 60th*, volume 1, pages 225–229. IEEE, 2004.
- [11] SS Suh, WL Stutzman, WA Davis, Alan Waltho, and J Schiffer. A novel printed dual polarized broadband antenna, the fourclover antenna. *Proceeding of the international symposium on antenna and Propagation, ISAP 2004, Sendai, Japan*, pages 77–80, 2004.
- [12] Seong-Youp Suh, Warren Stutzman, William Davis, Alan Waltho, and Jeffrey Schiffer. A generalized crossed dipole antenna, the fourtear antenna. In *Antennas and Propagation Society International Symposium, 2004. IEEE*, volume 3, pages 2915–2918. IEEE, 2004.
- [13] Martin Leung. *A Wideband Feed for A Cylindrical Radio Telescope*. PhD thesis, University of Sydney, 2008.
- [14] J.G. Robertson. The most and other raido telescopes. *Aust. J. Phys.*, 44:729, 1991.
- [15] Stephen D. Gedney. *Introduction to the Finite-Difference Time-Domain Method for Electromagnetics*. Synthesis Lectures on Computational Electromagnetics. Morgan and Claypool, 2011.
- [16] Constantine A. Balanis. *Antenna Theory: Analysis and Design*. John Wiley And Sons, Inc., Hoboken, 2005.
- [17] David M. Pozar. *Microwave Engineering*. John Wiley And Sons, Inc, 2005.
- [18] Yunqiang Yang, Y Wang, and Aly E Fathy. Design of compact vivaldi antenna arrays for uwb see through wall applications. *Progress In Electromagnetics Research*, 82:401–418, 2008.
- [19] Ehud Gazit. Improved design of the vivaldi antenna. In *IEE Proceedings H (Microwaves, Antennas and Propagation)*, volume 135, pages 89–92. IET, 1988.

Appendix

The Cloverleaf Antenna: A Compact Wide-bandwidth Dual-polarization Feed for CHIME

Meiling Deng^a and Ducan Campbell-Wilson^b for the CHIME collaboration

^aDepartment of Physics and Astronomy, The University of British Columbia, Email: mdeng@phas.ubc.ca

^bSchool of Physics, The University of Sydney, Email: dcw@physics.usyd.edu.au

Abstract—We have developed a compact, wide-bandwidth, dual-polarization cloverleaf-shaped antenna to feed the CHIME radio telescope. The antenna has been tuned using CST to have smaller than -10dB s_{11} for over an octave of bandwidth, covering the full CHIME band from 400MHz to 800MHz and this performance has been confirmed by measurement. The antennas are made of conventional low loss circuit boards and can be mass produced economically, which is important because CHIME requires 1280 feeds. They are compact enough to be placed 30cm apart in a linear array at any azimuthal rotation.

Keywords: antenna, dual polarization, wide bandwidth, radio telescope

I. INTRODUCTION

We have built a novel, cloverleaf shaped compact dual-polarization feed for the Canadian Hydrogen Intensity-Mapping Experiment [1]. CHIME is a radio telescope designed to measure Baryon Acoustic Oscillations (BAO) by measuring the intensity of neutral hydrogen over half the sky through the redshift range $0.8 \leq z \leq 2.5$. At these redshifts the 21cm line of neutral hydrogen appears in the frequency range 400MHz to 800MHz . CHIME has no moving parts; it consists of five parallel cylindrical parabolic reflectors, each 20m wide, 100m long and $f/0.25$. Feeds are spaced 30cm apart along each focal line. Signals are amplified and brought to a single custom digital correlator.

The full instrument requires 1280 dual polarization feeds with an acceptable beam pattern, low material loss and s_{11} lower than -10dB from 400MHz to 800MHz . With this many feeds, it is important that uniform, reliable feeds can be manufactured economically. Other solutions considered as CHIME feeds are the four-square antenna [2] [3] developed for the Molonglo Telescope [4], the four-point antenna [5] and the four-point antenna with tuning plate [6]. All these feeds generate an approximately circular beam suitable for feeding deep paraboloidal reflectors. The performance of these feeds differs mostly in their matching bandwidth.

II. RADIATION MECHANISM

Our feeds are a modification of four-square antennas developed for the Molonglo Observatory. The petals, stem and base are all made from printed circuit boards (PCB). To broaden the bandwidth, we have modified the petals to have curved outer edges as shown at left in Figure 1, eliminating the dependence on a single dimension. The curves are smooth and each petal is symmetric. CST simulated current pattern is shown at right in Figure 1 for one linear polarization at 600MHz . The currents near the gaps between petals run in opposing directions so they cancel, and do not contribute to the radiation pattern. For this polarization, farfield radiation

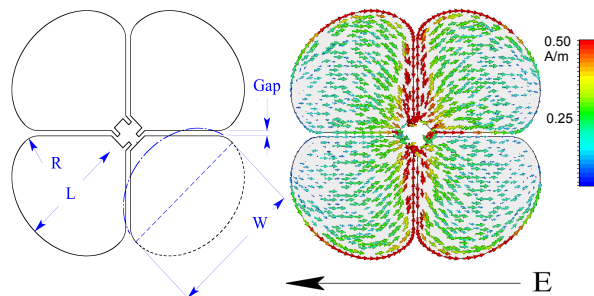


Fig. 1. At left, the shape of each petal consists of two perpendicular straight lines, two 45 degree circular arcs with radius R and one half an ellipse. W is the major axis of the ellipse and L is the length from the intersection of the straight sides to the outer edge of the ellipse. The shape is illustrated here for the adopted values of gap, R , L , and W . Each of the four tabs shown at the centre is connected to one side of a vertical microstrip transmission line and in each case the full width of the adjacent petal is connected to the other lead. At right, CST simulated currents for one linear polarization at 600MHz are shown. Note the small asymmetry in the current distribution near the centre because of the tab geometry.

arises from the coherent currents running along the curved outer edges of the top and bottom pair of petals. For each linear polarization, two differential signals, each from a pair of petals, are combined through tuned baluns to form one single-ended output. Thus each single polarization signal involves currents in all four petals. This is called in-pair feeding. Full baluns, from both polarizations, consist of four identical microstrip transmission lines along four vertical support boards (stem) and a horizontal base board. Both of the single-ended outputs are on the base board. Each transmission line is varied in several abrupt steps, and the lengths and characteristic impedances of the transmission line segments are tuneable. We have demonstrated that electrical losses in conventional circuit board materials generate unacceptable noise levels for astronomical instrumentation. Teflon-based PCB is used everywhere there is a transmission line.

III. TUNING THE ANTENNA PERFORMANCE

In order to tune the antenna parameters to produce acceptable performance we have constructed a full CST model of a cloverleaf antenna (only one polarization present). To verify the procedure, we first built two different cloverleaf antennas with arbitrarily chosen shapes, measured their s_{11} and compared these measurements to CST simulations. The comparison proves our CST simulation is reliable.

Measurements show that coupling between two polarizations and coupling between adjacent antennas do not affect s_{11} . Therefore, we proceeded to iterate the cloverleaf design using CST following the plan listed below.

We initially fixed the parameters of the transmission lines to a design chosen for ease of manufacture: the transmission line has two characteristic impedances, one on the vertical support board and the other on the horizontal baseboard.

We set the initial petal parameters to be $(R, W, L) = (80, 140, 150)$ mm and altered R, W , and L successively, to learn which parameters have the most impact on the antenna's s_{11} . Altering R has very little impact, and we fixed it to $R = 20$ mm, the peak of a very shallow performance curve.

We used the optimization algorithm implemented in CST to explore s_{11} in (W, L) space. Varying W and L simultaneously until CST finds the smallest s_{11} across the band. Optimization was still running after two days and we manually stopped it.

We found that for these transmission lines and for $R = 20$ mm, s_{11} has strong dependence on W and L . However, all s_{11} curves pass through an apparent fixed point at approximately $f = 580$ MHz, $S_{11} = -12$ dB. From this result and from a manual exploration of transmission line impedance we concluded that this optimization step is essentially minimizing s_{11} by matching the petal shape to the fixed balun parameters.

We introduced an additional degree of freedom by dividing the vertical portion of the transmission line from one segment to two segments with different impedances. From among more than 60 sets of parameters returned by CST, we picked $(W, L) = (138.5, 131.9)$ mm which has the smallest s_{11} across the band although it does not meet our specifications and explore transmission line properties. We held total length of vertical transmission line fixed to ensure $\frac{1}{4}\lambda$ separation between radiating petals and reflective ground plane, and varied characteristic impedances and the step location.

With the upper trace width 3.5mm, length 92mm and lower trace width 2.5mm, length 40mm, the result is dramatic. The fixed point is removed and the s_{11} is below -15dB across the band except for near 400MHz, where we just meet our requirement of -10dB.

We stopped our tuning procedure at this point. Although a solution has been found which exceeds our requirements, the system has not been optimized. Petal shape parameters and transmission line parameters have been varied separately but the full space of these parameters has not been explored. We can use this in future work to add additional performance criteria to the design procedure.

IV. RESULTS

Four petals of the chosen shape are built into one piece of double-sided PCB with FR4 as substrate to save cost. Vias connect the two copper surfaces to reduce material loss in FR4. The circuit boards are slotted to remove FR4 in the gaps between petals because leaving FR4 in the gaps has a serious effect on both antenna impedance and material losses. Note that the resulting petal size and shape are compatible with 45 degree azimuthal rotation in an array. The s_{11} of an assembled feed is shown in Fig. 2 for both polarizations and in comparison with simulations. According to simulation, the beam pattern is smooth in both the E-plane and the H-plane. HPBW varies within several degrees across the band. The six PCB pieces of the cloverleaf antenna are soldered together using a mechanical jig. A photo of eight antennas in a linear

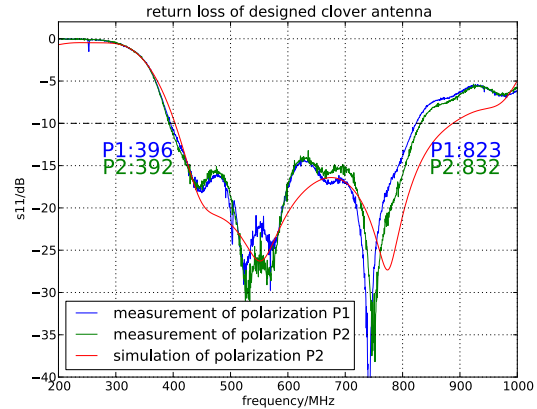


Fig. 2. The measured s_{11} spectrum for both linear polarizations is plotted along with the CST simulation. Note the similarity between two polarizations. This design exceeds the requirement of $S_{11} \leq -10$ dB over the full band from 400 to 800 MHz.



Fig. 3. A linear array of eight cloverleaf antennas installed at the focal line of the CHIME Pathfinder at the Dominion Radio Astrophysical Observatory in Penticon, BC, Canada. The picture is taken through the wire mesh reflective surface (mesh spacing 19 mm) illustrating a photonsview of the antennas and ground plane. Notice that each feed has an image-feed in the ground plane, $\frac{1}{2}\lambda$ away at the passband centre frequency. Notice also the four slots cut to remove dielectric material from the gaps between the petals.

array installed on the CHIME pathfinder is shown in Fig.3.

V. ACKNOWLEDGEMENTS

CHIME is funded by the four partner institutions, grants from NSERC and the Canada Foundation for Innovation. MD acknowledges support from MITACS. DCW acknowledges support from Sydney University for this work.

REFERENCES

- [1] CHIME is a partnership between UBC, McGill, UToronto and the DRAO. <http://chime.physics.ubc.ca>
- [2] Martin Leung (2008), "A Wideband Feed for a Cylindrical Radio Telescope", Ph.D thesis, University of Sydney
- [3] C. Buxton;W. Stutzman;and J. Nealy, "Implementation of the Foursquare antenna in broadband arrays", URSI National Radio Science meeting, July 1999. (Paper 99-12)
- [4] J.G. Robertson, "The MOST and Other Radio Telescopes", Aust. J. Phys. 1991, 44, 729
- [5] Seong-Youp Suh; Stutzman, W.L.; Davis, W.A., "Low-profile, dual-polarized broadband antennas", Antennas and Propagation Society International Symposium, 2003.
- [6] Seong-Youp Suh; Stutzman, W.L.; Davis, W.A.; Waltho, A.E.; Skeba, K.W.; Schiffer, J.L., "Bandwidth improvement for crossed-dipole type antennas using a tuning plate", Antennas and Propagation Society International Symposium, 2005.